https://doi.org/10.5194/egusphere-2026-2550
Preprint. Discussion started: 26 May 2026

Long-term BVOC Fluxes in a Suburban Tokyo Forest: Insights from Integrated Drone and Tower Observations

Yujiro Ichikawa[*1], Katsuhito Yoshida[2], Shinichi Yonemochi[1], Kentaro Takagi[3], Atsuyuki Sorimachi[2], Kazuhide Matsuda[4], Toshimasa Ohara[5]

[1]Center for Environmental Science in Saitama, 914 Kamitanadare, Kazo City, Saitama, 347-0115, Japan,
[2]Toyo University, 2100 Kujirai, Kawagoe City, Saitama, 350-8585, Japan
[3]Hokkaido Univesity, Aza Tōkanbetsu, Horonobe Town, Teshio District, Hokkaido, 098-2943, Japan
[4]Tokyo University of Agriculture and Technology, 1528 Horinouchi, Hachioji City, Tokyo, 192-0355, Japan
[5]Asia Center for Air Pollution Research, 1182 Sowa Nishi-ku, Niigata City, Niigata, 950-2144, Japan

Correspondence to: Yujiro Ichikawa (ichikawa.yujiro@pref.saitama.lg.jp)

Abstract. Biogenic volatile organic compounds (BVOC) substantially impact regional photochemical air pollution, global climate change, and the carbon cycle. Although research on BVOC emissions is of paramount importance, only few studies have measured long-term BVOC fluxes from forest ecosystems. There are no long-term observational studies on BVOC emissions from suburban forests of major cities in Asia under a humid subtropical climate, which may have a major impact on urban air quality. We conducted long-term, multi-height BVOC observations at a 30 m flux tower in suburban Tokyo, evaluating isoprene emission flux from a *Quercus serrata* dominated mixed forest using the aerodynamic gradient method. Spatial variability was examined through integrated drone and tower observations, and Model of Emission Gases and Aerosols from Nature (MEGAN) estimates were compared with measurements. Isoprene volume mixing ratios increased significantly during the warm season (May–October), accounting for over 90% of BVOC composition in peak summer, while monoterpenes remained low with minimal vertical gradients. Isoprene exhibited distinct vertical volume mixing ratio gradients peaking within the canopy, with daily average emission flux ranging from −0.05 to 15.30 $mg \cdot m^{-2} \cdot h^{-1}$. Horizontal volume mixing ratio variability within 30 m reached 10–30%, with enhanced heterogeneity in summer. Horizontal flux differed by approximately 30% between tower (height: 23–30 m) and drone (30–40 m) measurements. MEGAN systematically overestimated observations with maximum deviations in summer. These findings, derived from long-term observations, will contribute to assessing the impact of BVOCs on air quality and climate in cities worldwide, beyond temperate humid regions of Asia, and to reducing model uncertainties.

Keywords: BVOC, Isoprene, Emission, Flux measurements, Drone, Tower, MEGAN

1. Introduction

https://doi.org/10.5194/egusphere-2026-2550
Preprint. Discussion started: 26 May 2026

Terrestrial vegetation contributes to the release of large amounts of biogenic volatile organic compounds (BVOCs) into the atmosphere. BVOCs comprise dozens to hundreds of chemical species, including terpenoids, alkanes, alcohols, carbonyls, esters, ethers, and fatty acids (Penuelas and Llusià, 2004; Tani and Mochizuki, 2021; Yang et al., 2020). Although the detailed mechanisms regarding why terrestrial vegetation emit BVOC remain incompletely understood, these compounds are generally thought to be emitted as part of defense systems against abiotic stresses such as heat and biotic stresses such as insects and pathogens (Celedon and Bohlmann, 2019). Furthermore, some studies suggest that BVOC function as signaling molecules for terrestrial vegetation (i.e., allelopathy) to transmit defense signals to surrounding plants when facing biological stress (Ninkovic et al., 2020; Sharifi and Ryu, 2020).

BVOC emission patterns from terrestrial vegetation vary significantly by species and are broadly categorized into the following four types: Type A, in which BVOC biosynthesis and emission occur simultaneously, is widely observed in broad-leaved trees and herbaceous plants. Type B, in which biosynthesized BVOCs are stored within leaves, branches, and roots before being emitted, is widely observed in conifers and herbaceous plants. Type C exhibits characteristics of both Type A and Type B, while Type D emits little to no BVOCs (Okumura, 2021; Tani and Mochizuki, 2021; Tani et al., 2024). Regarding BVOC emission intensity, Type A species often exhibit both temperature and solar radiation dependences, while Type B species typically show only temperature dependencies.

Among the chemical species of BVOCs, terpenoids account for a large proportion of emissions. Terpenoids primarily include isoprene (C_5H_8), monoterpenes ($C_{10}H_{16}$), sesquiterpenes ($C_{15}H_{24}$), and others. The estimated global annual emission of BVOCs is 1,150 $TgC \cdot yr^{-1}$, of which isoprene accounts for 503 $TgC \cdot yr^{-1}$ (47% of annual emission) and monoterpenes for 127 $TgC \cdot yr^{-1}$ (11%) (Guenther et al., 1995). According to estimates based on vegetation type, trees as the primary source account for approximately 821 $TgC \cdot yr^{-1}$ (71% of annual emission). Needleleaf trees, broadleaf trees, shrubs, grass, and crops each account for 10–30% of the global terrestrial vegetation cover area. Among these, broadleaf trees are estimated to contribute approximately 80% of total BVOC emissions (Guenther et al., 2013).

Many terpenoids exhibit high reactivity with atmospheric reactive species such as hydroxyl radicals (Atkinson and Arey, 2003), with isoprene and monoterpenes having atmospheric lifetimes ranging from tens of minutes to several hours. They significantly contribute to the formation of photochemical pollutants such as tropospheric ozone (O_3) and secondary organic aerosols (SOA). O_3 and aerosols adversely affect human health and contribute significantly to climate change. Specifically, O_3 promotes warming, while aerosols have both absorbing and scattering properties that overall suppress warming (IPCC, 2021). Furthermore, 3−15% of the carbon fixed within plants through photosynthesis is released as isoprene (Tani and Kawawata, 2008). Thus, BVOCs play a significant role in photochemical air pollution, climate change, and the carbon cycle. Consequently, research on BVOC emissions and atmospheric chemistry is of paramount importance for air quality management and climate change mitigation efforts.

In large urban areas with limited vegetation, one might assume that BVOCs have little or no impact on air quality. Using a model, Situ et al. (2013) found that BVOCs emitted primarily from outside the Pearl River Delta region in China during the autumn of November contributed an average of 7.9 ppb and a maximum of 24.8 ppb to O_3 volume mixing ratios in the

https://doi.org/10.5194/egusphere-2026-2550
Preprint. Discussion started: 26 May 2026

region, including urban areas downwind. In Berlin, a city renowned for its abundance of green spaces among European cities, the average contribution of BVOCs to O_3 was estimated by the model to peak in July, at 17–20% (Churkina et al., 2017). In Japan, it has been reported that approximately 14.1 ppb of the O_3 generated in Tokyo during the summer is attributable to BVOCs (Chatani et al., 2015). Furthermore, Nishimura et al. (2015) state that 10.3 ppb (15.9%) of the daily maximum O_3 volume mixing ratio in Osaka (Japan's second-largest city after Tokyo) is attributable to BVOCs from forested areas in the surrounding regions. These model studies suggest that forests surrounding major cities may serve as crucial upwind sources of reactive BVOCs. It is, therefore, essential to ascertain the actual emission levels from these forested areas. Research on BVOC emissions from forests plays a crucial role in elucidating the relationship of these emissions with urban air quality. Furthermore, accurate emission data are required to improve the accuracy of model calculations.

Numerical simulation models are primarily used to quantitatively evaluate the impact of chemical emissions on air quality by simulating physicochemical mechanisms such as reactions, transport, and deposition. The Model of Emissions of Gases and Aerosols from Nature (MEGAN), which is used to estimate BVOC emission fluxes from terrestrial vegetation, uses standardized basal emission rates as an input parameter (Guenther et al., 2006, 2012). However, the majority of basal emission rate measurements rely on enclosure methods applied to individual branches and leaves, and due to the difficulty of accessing different layers of the canopy, they do not fully capture the actual BVOC emissions from the entire tree canopies. In addition, it has been reported that stress factors, such as physical impact or damage to branches or leaves can increase the emission rates of BVOCs (Jutti, 1990), resulting in high measurement uncertainty depending on the conditions used in the enclosure method. Furthermore, considering that basal emission rates vary across canopy layers due to environmental differences (such as temperature and solar radiation), scaling from individual branch and leaf measurements to canopy scale fluxes likely involves significant uncertainty. Micro-meteorological methods can directly measure flux within canopy scales. This approach generally utilizes flux towers extending above the upper canopy layer, enabling realistic and reliable measurements without disturbing the vegetation (Tani et al., 2024; Guenther et al., 2006). Reportedly, BVOC emissions scaled up from the branch and leaf scales to the canopy scale do not correspond to those obtained using micro-meteorological methods (Bai et al., 2025).

Numerous studies utilized micro-meteorological methods for BVOC flux observations in various countries and forest types (Bai et al., 2016; Bai et al., 2025; Baker et al., 2005; Bouvier-Brown et al., 2012; Dumont et al., 2026; Emmerson et al., 2016; Fares et al., 2013; Fuentes and Wang, 1999; Fuentes et al., 1999; Holzinger et al., 2006; Ieda et al., 2006; McKinney et al., 2011; Miyama et al., 2013; Mochizuki et al., 2014, 2015, 2020; Räisänen et al., 2009; Rantala et al., 2016; Seco et al., 2017; Situ et al., 2013; Wei et al., 2018). Although recent studies on BVOC emphasize the need to understand actual seasonal variations in BVOC emissions (Chatani et al., 2022) and to conduct long-term flux observations (Bai et al., 2025; Tani and Mochizuki, 2021), many flux observations conducted worldwide are limited to periods ranging from a few days to less than a year, resulting in a lack of seasonal or annual assessments, making the results unrepresentative. Very few long-term observations of BVOC fluxes using towers have been conducted for more than a year (e.g., Bouvier-Brown et al., 2012; Dumont et al., 2026; Rantala et al., 2016). In Japan, only Mochizuki et al. (2014) conducted a one-year monoterpene flux

https://doi.org/10.5194/egusphere-2026-2550
Preprint. Discussion started: 26 May 2026

observation in the *Larix kaempferi* forest at the Fuji-Hokuroku Flux Research Site. Although long-term flux measurements using micro-meteorological methods at BVOC emission sources in suburban areas are crucial for gaining a better understanding of and estimating the impact of BVOCs on urban air quality, such studies are extremely rare. Rantala et al. (2016) conducted flux measurements for over a year in the background forest area of Helsinki, Finland, which has a subarctic climate. However, to the best of our knowledge, no such studies have been conducted in the suburbs of major cities in Asia under a humid subtropical climate. Therefore, in this study, we conducted observations over a long period of two and a half years in a forest area in the suburbs of Tokyo, to clarify the actual BVOC emission levels. As scientific knowledge regarding BVOC emissions from forested areas in suburban settings is relevant not only in Japan but also in similar environments around the world, this study serves as an important case study. Furthermore, most flux observations rely on single fixed towers, with limited assessment of spatial representativeness and horizontal heterogeneity, particularly in complex suburban forest environments.

This study involved multi-height observations of BVOCs and measured emission flux using the aerodynamic gradient method (AGM), one of the micrometeorological techniques, at a flux tower installed in a research forest in the Tokyo metropolitan area, Japan, located within a humid subtropical climate zone, over a period of approximately two and a half years, from June 2023 to October 2025. By integrating aerial observations using multi-rotor unmanned aerial vehicles (UAV, commonly known as drones) with fixed-point observations around the flux tower, we further assessed the spatial variability of measurements obtained from a single flux tower. In addition, by comparing the observational data with estimates from the MEGAN model, we evaluated model performance and characterized sources of uncertainty. Comparative analyses between long-term observational data from suburban areas and the MEGAN model are rare, making these findings particularly valuable. The uniqueness of this study lies in the fact that it involved long-term, on-site assessments of the temporal and spatial variability of BVOCs in suburban forest areas, which directly affect urban air quality, as well as comparisons between model predictions and observed datasets. Specifically, we address three key questions: (1) What is the seasonal and interannual variability of BVOC emissions in a suburban Tokyo Forest? (2) What is the magnitude of spatial heterogeneity in BVOC volume mixing ratios and fluxes? (3) How well does MEGAN reproduce observed emissions, and what are the primary sources of model-observation discrepancy?

2. Methods

2.1 Site description

This study was conducted at the Field Museum Tamakyuryo (FM Tama), a research forest facility of Tokyo University of Agriculture and Technology located in the western suburb of Tokyo (35°38′18″N, 139°22′41″E), as shown in Fig. S1. A 30 m high scaffold flux tower has been constructed on the floor of FM Tama (168 above sea level). This site has been extensively used to conduct numerous atmospheric observational and micro-meteorological studies (e.g., Matsuda et al., 2015; Xu et al., 2021). Details regarding the FM Tama are described in Matsuda et al. (2015), but are briefly outlined below. The site covers approximately 20 hectares. The area around the flux tower is dominated by the deciduous tree *Quercus*

https://doi.org/10.5194/egusphere-2026-2550
Preprint. Discussion started: 26 May 2026

serrata, and the needleleaf tree *Japanese cedar* is also sparsely scattered in small numbers throughout other parts of the site, creating a mixed forest character. The trees reach heights of approximately 20 m, with the canopy layer distributed between 10–20 m above ground level. *Q. serrata* began to grow lush foliage around April and had shed its foliage by around November to December. In contrast, *J. cedar* is an evergreen tree and generally does not shed its leaves. The *J. cedar* trees at FM Tama are estimated to be approximately 50 years old (Naemura et al., 2003), and the *Q. serrata* trees are also presumed to be roughly the same age.

The wind rose for the observation period described in Section 2.2 is shown in Fig. S2. Prevailing winds are predominantly southerly, followed by northerly winds, then easterly winds, with westerly winds being rare. Consequently, the wind rose indicates that no major BVOC emission sources exist upstream outside the research forest, suggesting that the BVOC components detected at the flux tower primarily originate from FM Tama. Meanwhile, although Naganuma Park, a forest park, lies west of the flux tower, its influence is considered negligible.

2.2 Sampling period

BVOC sampling was conducted for 1–3 days each month from June 2023 to October 2025, though there were months when measurements could not be performed due to equipment maintenance or power outages. The observation dates and representative meteorological data for those days are shown in Table S1; rainy days are not included. In this paper, all times are expressed in Japanese standard time (JST, UTC+9).

2.3 Meteorological observations

A 3-dimensional ultrasonic anemometer (YOUNG, 81000) installed at the flux tower top of 30 m measured horizontal and vertical wind direction and speed, as well as virtual temperature, and data were averaged over 10–30 min intervals. Additionally, an integrated weather sensor (VAISALA, WXT520) was installed at the flux tower heights of 25 m, 20 m, 17 m, and 1 m from June 2023 to November 30, 2023, and at 30 m, 24 m, 20 m, 17 m, 10 m, and 2 m from February 22, 2024 to October 2025 to measure air temperature, relative humidity, and horizontal wind direction and speed (Climatec CVS-HMP110 thermo-hygrometers and Climatec CYG-91000 anemometers were also used for some periods). The 10-min averages were used to obtain vertical profiles of each parameter. In cases where meteorological data could not be acquired at the flux tower due to maintenance or other reasons, measurements from the nearest Hachioji air quality monitoring station, which is managed by the Tokyo metropolitan government, were used.

Solar radiation including photosynthetic photon flux density (PPFD) was measured at 10-min intervals using a pyranometer (PREDE, PCM-01N) at 30 m height of the flux tower. The leaf area index (LAI) around the tower was measured for 1–3 d per month using a plant canopy analyzer (LI-COR LAI-2200), and the average value from multiple locations was used.

2.4 BVOC sampling and measurement

https://doi.org/10.5194/egusphere-2026-2550
Preprint. Discussion started: 26 May 2026

Based on the previously reported BVOC measurement conditions (Ichikawa et al., 2023), isoprene and seven monoterpenes (α/β-pinene, camphene, myrcene, 3-carene, limonene, p-cymene) were selected as target substances for measurement. BVOC samples were collected using an in-house sampling device shown in Fig. S3. Air samples entering through the atmospheric inlet passed through a dehumidification tube (FUJIFILM Wako Pure Chemical, magnesium perchlorate, elemental analysis grade, 6–14 mesh) and an ozone scrubber cartridge (FUJIFILM Wako Pure Chemical, Presep-C Ozone Scrubber, potassium iodide). The air was then divided into four flow paths using a PTFE manifold. Each flow path was connected to a sorbent tube, with a two-way solenoid valve connected downstream. The opening and closing of the valves were controlled by a 4-channel timer, enabling sample collection at different time intervals. All tubing was made of PTFE and the flow rate was set to 100 mL·min^{-1}.

The sampling devices were installed at heights of 30 m and 23 m above the canopy top, 17 m within the canopy, and 3 m near ground level, as shown in Fig. 1 (a). Sampling was conducted with a time resolution of 10–30 min during the period from 10:00 am– 4:00 pm (JST), typically four samples in the morning and four in the afternoon.

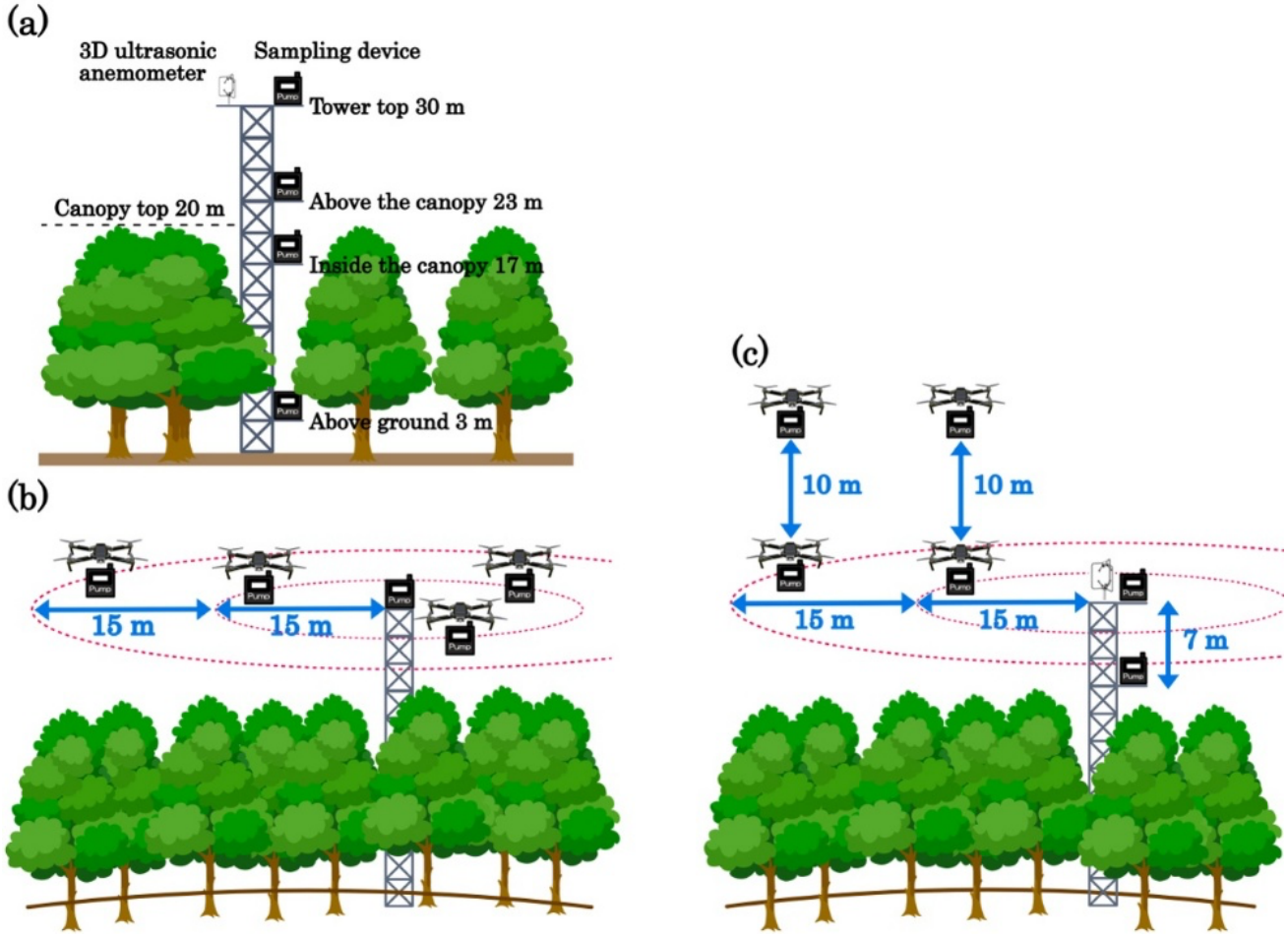

https://doi.org/10.5194/egusphere-2026-2550
Preprint. Discussion started: 26 May 2026

Figure 1: Schematic diagram showing the configuration of sampling equipment on the drone and flux tower, along with the observation points. (a) Observation method at multiple heights on the tower; (b) Method for observing horizontal volume mixing ratio **variations using the tower and drone; (c) Method for observing horizontal flux variations using the tower and drone.**

For the sorbent tube, Air Toxics (Camsco, multibed type packed with Carbograph and Carbosieve) was used from June 2023 to May 2024, and a manufacturer customized multibed type packed with Tenax TA and Carbotrap B (Camsco) was used from June 2024 to October 2025. Conditioning of the sorbent tubes was performed with a temperature program of 40°C (hold 1 min) →10°C·min^{-1}→350°C (60 min) in a thermostatic chamber modified from gas chromatography oven while high-purity nitrogen gas (>99.9999% purity) was flowing at a flow rate of 50 mL·min^{-1}. Immediately after conditioning, the sorbent tubes were tightly closed at both ends with a brass cap using PTFE sealer, placed in stainless-steel containers with activated carbon, and stored in a glass desiccator under vacuum until sampling.

After sample collection, the sorbent tubes were tightly capped at both ends with brass caps, sealed in a desiccator with activated carbon to prevent contamination in an air-conditioned, controlled room, and stored until further analysis. Sample measurement was performed within one month of sampling.

A travel blank was used to confirm the effects of contamination during sample transport and storage. The travel blank was analyzed using the same method as that for the actual samples, and its value was subtracted from the analysis value of the actual samples.

Based on the static dilution method described in the U.S. EPA published manual “TO-15A” (EPA, 2019), a fixed amount of each BVOC component standard solution dissolved in methanol (FUJIFILM Wako Pure Chemical, LCMS grade) was spiked into a clean inert stainless vacuum canister (GL Sciences, GL-Scan). The canister was then heated at 60°C for 2 h to completely vaporize the components. After returning to room temperature, the canister was pressurized with VOC-free high-purity nitrogen gas (>99.9999% purity) to create a BVOC mixed standard gas. Toluene-d_8 (FUJIFILM Wako Pure Chemical, NMR grade, 99.5% purity) was used as the internal standard gas and was prepared in the same manner as described above.

BVOC were analyzed using a gas chromatography–mass spectrometer (GC-MS; Shimadzu, GC-MS QP2010plus) connected to an automated thermal desorption system (PerkinElmer, TurboMatrix 650 ATD). Detailed measurement conditions are as described in previous study (Ichikawa et al., 2023). These devices undergo regular manufacturer inspections to ensure that they are in good condition and free of defects. The lower detection limit (3σ) was calculated from the standard deviation (σ) obtained from repeated measurements of the standard gas (n=5–7).

2.5 Flux calculation

According to Tani et al. (2024), *Q. serrata* emits isoprene but does not emit monoterpenes. As shown in the Section 3.1 below, volume mixing ratio of monoterpenes remained extremely low compared to isoprene, and sometimes fell below the detection limits. Considering that isoprene emission around the flux tower is primarily attributable to the dominant species *Q. serrata*, flux calculations were performed for isoprene only.

https://doi.org/10.5194/egusphere-2026-2550
Preprint. Discussion started: 26 May 2026

The aerodynamic gradient method (AGM) adopted in this study to determine isoprene emission flux is a fundamental method classically used to estimate flux of trace gas components. The flux calculation in AGM is defined by the following Eq. (1) in accordance with Fick's first law (Erisman and Draaijers 1995; Fuentes, 1999; Räisänen, T. et al., 2009; Hayashi, 2010; Matsuda et al., 2010).

$$F_{\mathrm{obs}} = -K \cdot \frac{\partial C}{\partial z} = -\frac{u_* \cdot \kappa \cdot (C_{\mathrm{u}} - C_{\mathrm{l}})}{ln\left(\frac{z_{\mathrm{u}} - d}{z_{\mathrm{l}} - d}\right) - \Psi_{\mathrm{h}}\left(\frac{z_{\mathrm{u}} - d}{L}\right) + \Psi_{\mathrm{h}}\left(\frac{z_{\mathrm{l}} - d}{L}\right)} \quad (1)$$

where, F_{obs} is the observed flux (mg·m^{-2}·h^{-1}), K is the eddy diffusion coefficient (m^2·s^{-1}), C represents concentration (μg·m^{-3}), z represents height (m), and the subscripts u and l denote two heights above the canopy (u > l). u_* is the friction velocity (m·s^{-1}), κ is the empirically determined von Karman constant (=0.41), Ψ_{h} is the integrated stability correction for heat, L is the Monin-Obukhov length and d is the displacement height (m). u_* and L were derived from micro-meteorological elements (e.g., horizontal and vertical wind speed, virtual temperature). The value of d was derived from the vertical wind profile measured at the FM Tama flux tower by Xu et al. (2021) (April–November: 16 m, December–March: 15 m).

Observations in this study were not conducted at night or in the early morning for the following considerations, and were primarily carried out between 10:00 am–4:00 pm. AGM is generally not suitable for atmospheric conditions with stable boundary layers and weak turbulence during nighttime or early morning hours, whereas daytime implementation is preferable when turbulence intensifies and vertical flows and concentration gradients emerge (Erisman and Draaijers 1995; Tani et al., 2024). The average (median) friction velocity for the entire period was 0.64 (0.60) m·s^{-1}. No data points fell below the threshold of 0.10 m·s^{-1}, which Räisänen et al. (2009) excluded from analysis as weak turbulence intensity. This indicates that sufficient turbulence intensity was maintained during 10:00 am–4:00 pm, and the prerequisites for the AGM were generally satisfied. Furthermore, since the emission of many BVOC components exhibit temperature and light dependence, emissions are higher during the day, with isoprene showing this tendency most prominently. Note that due to maintenance of the observation equipment, some data are missing from December 1, 2023, to February 22, 2024.

2.6 Drone measurements

This study utilized a multi-rotor drone (DJI, Matrice 350 RTK). Multi-rotor drone offers the advantages of vertical takeoff and landing (VTOL) capability without requiring a runway, stable hovering, excellent maneuverability, and lower operational costs compared to helicopters or airplanes. Furthermore, the majority of aircraft are equipped with lithium polymer (Li-Po) batteries, and it is extremely important that they do not emit any exhaust gases that could significantly impact atmospheric observation data. One disadvantage of atmospheric observation using drones is that, given current battery technology, flight times are limited to approximately 15–30 min when considering the payload of meteorological and atmospheric observation equipment and cameras mounted on the aircraft.

The swirling airflow generated by propeller rotation causes atmospheric turbulence. If the placement of sample intake ports and measurement devices is not carefully considered, this turbulence significantly impacts measurement accuracy and

https://doi.org/10.5194/egusphere-2026-2550
Preprint. Discussion started: 26 May 2026

precision. However, it has been pointed out that many previous studies using drones do not address countermeasures for this swirling airflow (Altamira-Colado et al., 2024). Based on computational results from a fluid model by McKinney et al. (2019) and verification results from preliminary experiment using an actual aircraft regarding swirling airflow, the sample inlet, dehumidification tube, ozone scrubber cartridge and sorbent tube were mounted on a titanium-based support extended above the aircraft (approximately 60 cm above the main body of aircraft), as shown in Fig. 2. This configuration minimizes the effects of swirling airflow and aircraft vibration on the sample.

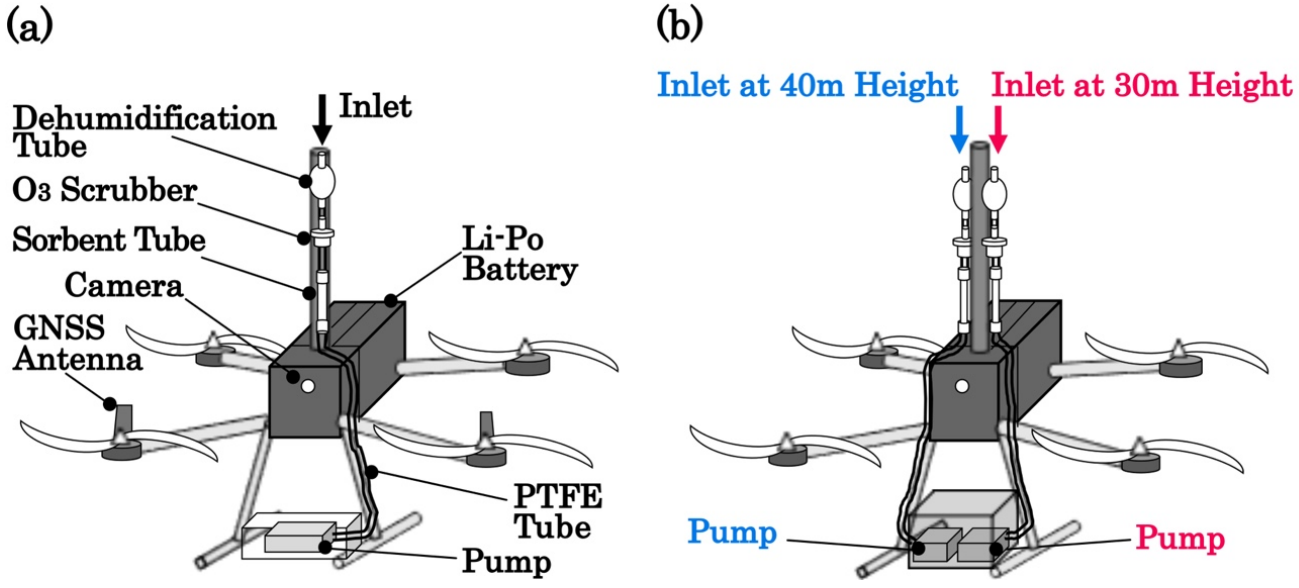

Figure 2: Status of equipment installed for BVOC sampling using a drone. (a) Installation for horizontal volume mixing ratio variations, (b) Installation for horizontal flux variations.

For the autumn season on October 12, 2023, and for the summer seasons on July 23, 2024, and June 17, 2025, parallel observations were conducted at the same height (30 m) using the drone and the flux tower at four locations approximately 15–30 m horizontally away from the flux tower (with differing azimuths), as shown in Fig. 1 (b), to evaluate the variability in volume mixing ratio in the horizontal direction. The flight position was determined by acquiring positional data via the Global Navigation Satellite System (GNSS) antenna, and was also constantly monitored visually from the flux tower. After arriving at the observation point, the aircraft hovered for a while to ensure stability before initiating sampling using the pump timer function. The stability of the drone at its fixed position during hovering is shown in Fig. S4. The drone equipment mounting method for these observations is as shown in Fig. 2 (a), and the observation time was set to 15 min. The flight altitude was precisely measured relative to the tree canopy using its onboard altitude sensor.

Furthermore, on July 29, 2025, during the summer season, spatial variability of the emission flux was evaluated using drone and flux tower, as shown in Fig. 1(c). Specifically, we calculated flux using the AGM equation presented in Section

https://doi.org/10.5194/egusphere-2026-2550
Preprint. Discussion started: 26 May 2026

2.5, based on observation results from two drone heights (30 m and 40 m) and two heights at flux tower (23 m and 30 m). Due to safety concerns, the drone did not collect samples at altitudes below 30 m, so the altitude differs from that of the tower. The drone had weight restrictions, preventing the installation of a 3-dimensional ultrasonic anemometer. Therefore, this study utilized data obtained from the flux tower, based on the assumption of the gradient method that both observation heights belong to the constant flux layer, and that there are no significant differences in micro-meteorological parameters. The configuration of equipment installed for this observation is shown in Fig. 2 (b), carrying two pumps and other equipment. After completing the first sampling at a height of 30 m at the observation point, the aircraft ascended vertically to 40 m and performed another sampling.

2.7 Isoprene emission estimation model

We compared the observed isoprene emission flux with model calculations from MEGAN (Guenther et al., 2006, 2012), an extensively used BVOC emission estimation model, to evaluate its applicability and reproducibility. The calculation period for this study was set from June 1, 2023 to October 31, 2025 to cover the actual observational period.

PPFD, meteorological elements and LAI data were obtained by the method described in Section 2.3. We estimated isoprene emission from *Q. serrata* at a 10-min time resolution. The estimation of isoprene emission flux F_{cal} ($mg \cdot m^{-2} \cdot h^{-1}$) was performed using the following Eq. (2), with parameters set based on the original literature for MEGAN (Guenther et al., 2006, 2012).

$$F_{cal} = \varepsilon \cdot \gamma_P \cdot \gamma_T \cdot \gamma_{LAI} \cdot \gamma_{age} \cdot \gamma_{SM} \cdot \gamma_{CO_2} \cdot \rho \quad (2)$$

where, ε is the basal emission rate under standard conditions for the plant functional type (PFT), and we adopted the value of 10 $mg \cdot m^{-2} \cdot h^{-1}$ for isoprene from broadleaf deciduous temperate tree. The standard conditions for MEGAN are described in Guenther et al. (2006, 2012); for example, a leaf temperature of 30°C, PPFD of 1500 $\mu mol \cdot m^{-2} \cdot s^{-1}$, and a standard canopy structure (LAI_{std}) of 5. Note that while a PPFD of 1000 $\mu mol \cdot m^{-2} \cdot s^{-1}$ was typically used as the standard condition at the leaf level for the G93 model (Guenther et al., 1993), a PPFD of 1500 $\mu mol \cdot m^{-2} \cdot s^{-1}$ is used in MEGAN at the canopy scale. Furthermore, the γ variables represent activity factors related to various environmental conditions, where γ_P represents light dependency, γ_T represents temperature dependency, γ_{LAI} represents LAI, γ_{age} represents leaf age, γ_{SM} represents soil moisture response, and γ_{CO_2} corresponds to the carbon dioxide response. ρ represents the escape efficiency, which is the proportion of isoprene emitted from the canopy that escapes into the upper atmosphere and the value of 0.96 was used Guenther et al. (2006). The setting of activity factors related to environmental conditions used in MEGAN is explained in the supplement S1.

The correspondence and error characteristics between the obtained calculated value F_{cal} and the observed isoprene emission flux F_{obs} were evaluated. To calculate the degree of systematic overestimation or underestimation of the model, the mean error bias (MEB) was determined using Eq. (3) as follows:

$$MEB = \frac{1}{N}\sum_{i=1}^{N}(F_{cal,i} - F_{obs,i}) \quad (3)$$

https://doi.org/10.5194/egusphere-2026-2550
Preprint. Discussion started: 26 May 2026

where N is the number of data points used for comparison. A positive value indicates that model overestimates the observed values, while a negative bias indicates underestimation.

Furthermore, as a comprehensive indicator for evaluating the magnitude of model error, the root mean square error (RMSE) was calculated using Eq. (4) as follows:

$$\mathrm{RMSE} = \sqrt{\frac{1}{N}\sum_{i=1}^{N}(F_{cal,i} - F_{obs,i})^2} \quad (4)$$

The closer this statistical indicator approaches its minimum value of 0, the closer the calculated value approaches the actual measured value.

3. Results

3.1 Volume mixing ratio of BVOCs

Fig. 3 shows the stacked bar graph of the monthly average volume mixing ratios of eight BVOC components by height over a 3-year period. The numerical data for each component in each month are summarized in Table S2. Note that the average values mentioned in the following text refer to the period from 10:00 am–4:00 pm on the observation day. From November to April, volume mixing ratios of all components were generally low throughout the month, with no significant differences observed at different heights. Conversely, during the warmer period from May to October, isoprene volume mixing ratios exhibited extremely high levels, with differences also observed at different heights.

https://doi.org/10.5194/egusphere-2026-2550
Preprint. Discussion started: 26 May 2026

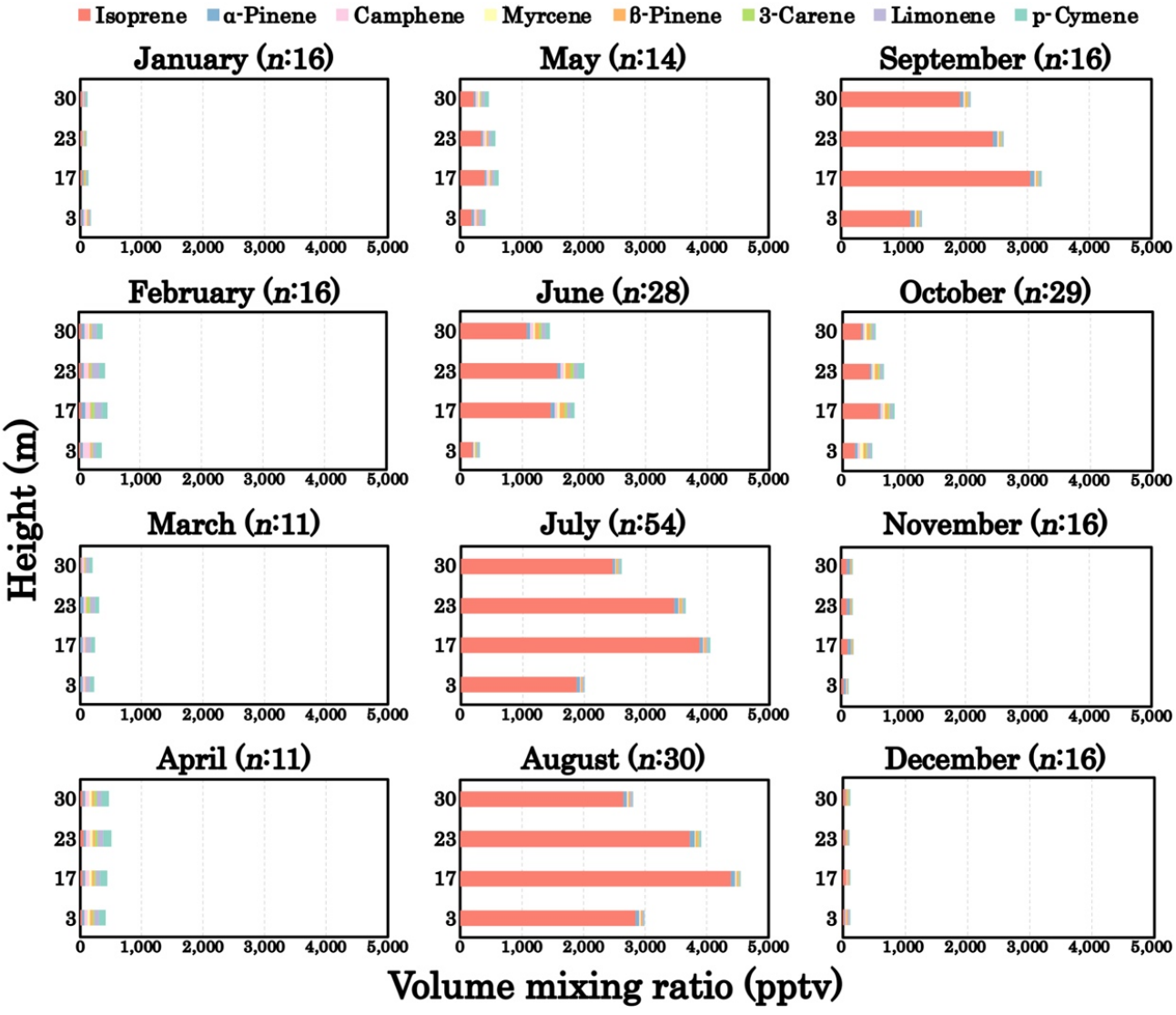

Figure 3: Stack bar chart of monthly average volume mixing ratios (pptv) of eight BVOC components by height over a 3-year period.

Isoprene volume mixing ratios began rising in May, peaking around July to August, with multiple samples exceeding 10,000 pptv. Fig. S5 shows the composition ratios of each component at different heights for each month. In July and August, isoprene accounted for over 90% of the total volume mixing ratio at all heights. Although the detailed mechanisms underlying isoprene emission in plants remain incompletely understood, the widely accepted explanation is that it protects leaves from high temperatures (Sharkey et al., 2008). This study also observed a tendency for isoprene volume mixing ratios to increase during periods of rising temperatures over the long observation period. As detailed in Section 3.2, an isoprene volume mixing ratio gradient forms between the canopy interior and exterior from this period onward.

https://doi.org/10.5194/egusphere-2026-2550
Preprint. Discussion started: 26 May 2026

Monoterpenes do not exhibit seasonal variations as pronounced as isoprene. While slight increases may be observed during summer, isoprene tends to dominate the volume mixing ratio to the overall composition. Among monoterpenes, α-pinene, limonene, and p-cymene showed relatively high volume mixing ratios, but each component accounted for only about 1–2% of the total volume mixing ratio during the summer, and the formation of volume mixing ratio gradients with height was also unclear. This result corresponds with Tani et al. (2024), indicating that *Q. serrata* is an isoprene-emitting species but releases almost no monoterpenes.

Through long-term atmospheric observations around the FM Tama flux tower, isoprene was confirmed to be a major component. Therefore, the following sections will focus on isoprene.

3.2 Vertical profile of isoprene

Fig. 4 shows the vertical distribution of isoprene at different heights for each month from January to December, using box plots and average values. The boxes represent the 25–75 percentile range, the whiskers represent the 2–98 percentile range, and the median and average are overlaid.

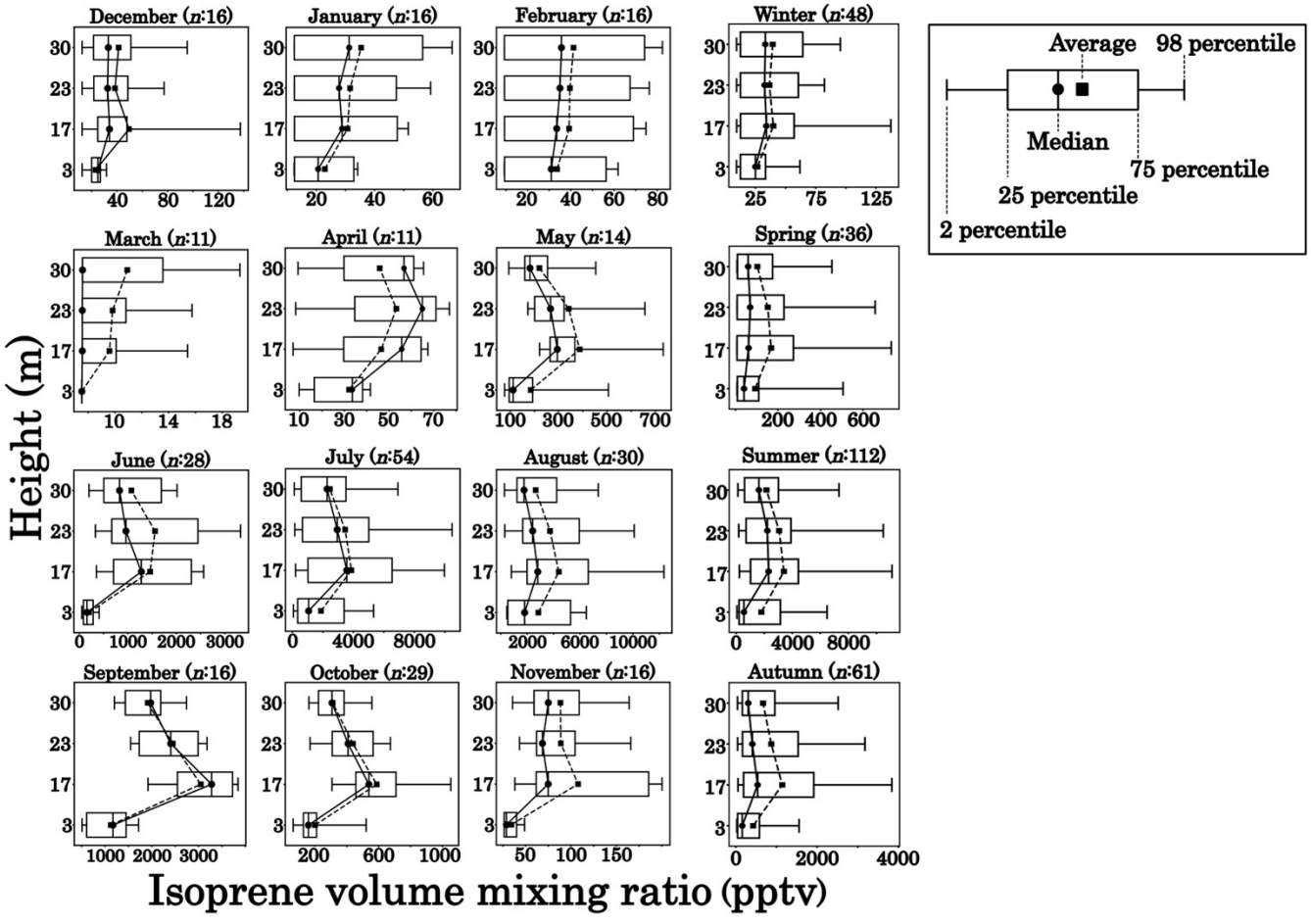

https://doi.org/10.5194/egusphere-2026-2550
Preprint. Discussion started: 26 May 2026

Figure 4: Boxplots overlaid with average values for the monthly and seasonal distribution of isoprene volume mixing ratios by height over a 3-year period. The solid and dashed lines connect the median and average values for each height, respectively.

345

The median and average values tended to be highest at 17 m, corresponding to the canopy interior, for many months. Particularly during the warm season (May to September) when *Q. serrata* leaves were densely foliated, the distribution at 17 m shifted toward higher volume mixing ratios (positive skewness), as evident from the x-axis scale of isoprene volume mixing ratios. This directly reflects that the primary source of isoprene emissions was located within the height range where 350 *Q. serrata* leaves were concentrated (the canopy range of 10–20 m). At 23 m and 30 m above the canopy, an increase in upper percentile values and a tendency toward a longer right tail in the distribution were also observed during the warm season. This suggests the existence of events where isoprene emitted from within the canopy is transported upward, leading to temporary high volume mixing ratios. Meanwhile, at 3 m, corresponding to the forest floor level, the median and average values were relatively lower throughout the year compared to other heights, and the distribution range was relatively 355 narrower. This suggests that the primary source of isoprene emissions is located within the canopy rather than at the forest floor. During the cold season (December to April), the distribution range narrowed across all heights. This reflects a state of significantly suppressed isoprene emissions, likely attributable to low temperatures, reduced solar radiation, and the phenology of *Q. serrata* leaf fall.

To more clearly illustrate seasonal variations, Fig. 4 also shows the vertical distribution of isoprene for each season. The 360 seasons are defined as follows: December through February is winter, March through May is spring, June through August is summer, and September through November is autumn. During winter, isoprene volume mixing ratios were extremely low at all heights, with a narrow distribution range. The median and average values were nearly identical, indicating low skewness in the distribution. Furthermore, no significant vertical gradient was observed between 17, 23, and 30 m heights. These results reflect a state where isoprene emission from *Q. serrata* was significantly low.

365 In spring, increases in the average values were observed at 17 m and a distinct vertical structure began to form compared to winter. Particularly at 17 m, the upper percentile values were higher than those at other heights, suggesting that the primary source of isoprene emission resided within the canopy. In contrast, volume mixing ratios at 3 m remained low with a narrow distribution range, indicating a limited contribution from the forest floor.

During summer, isoprene volume mixing ratios reached their highest levels among the four seasons. At 17 m, both the 370 median and average reached their maximum values, with the entire distribution significantly shifted toward higher volume mixing ratios. At 23 m and 30 m, the distributions clearly showed a positive skew with a long right tail in the distribution. This reflects that isoprene generated within the canopy is emitted as a net amount and undergoes vertical transport.

In autumn, although isoprene volume mixing ratios decreased than that in summer, a vertical structure centered around 17 m was observed. The median and average values were higher than those in the following winter, and the skewness of the 375 distribution also persisted. This indicates that although emission flux levels decreased with the drop in temperature and the onset of leaf fall, the primary source height for isoprene emission from within the canopy was maintained, a trend

https://doi.org/10.5194/egusphere-2026-2550
Preprint. Discussion started: 26 May 2026

particularly pronounced in September (autumn season). Meanwhile, the upper percentile values at 23 m and 30 m in autumn were less pronounced than those in summer, suggesting a decrease in the high emission events.

3.3 Isoprene emission flux observed at the tower

3.3.1 Trend over two and a half years based on observed values

Figure 5 shows the daily average isoprene emission flux (F_{obs}) calculated based on the vertical gradient of isoprene concentration ($\partial C/\partial z$) and the diffusion coefficient (K) at heights of 23 m and 30 m. Additionally, temperature inside the canopy, and PPFD during the observation period are overlaid (Fig. 5). The daily average values ± standard deviation for F_{obs} and related parameters are summarized in Table 1, with F_{obs} ranging from −0.05 to 15.30 mg·m^{-2}·h^{-1}.

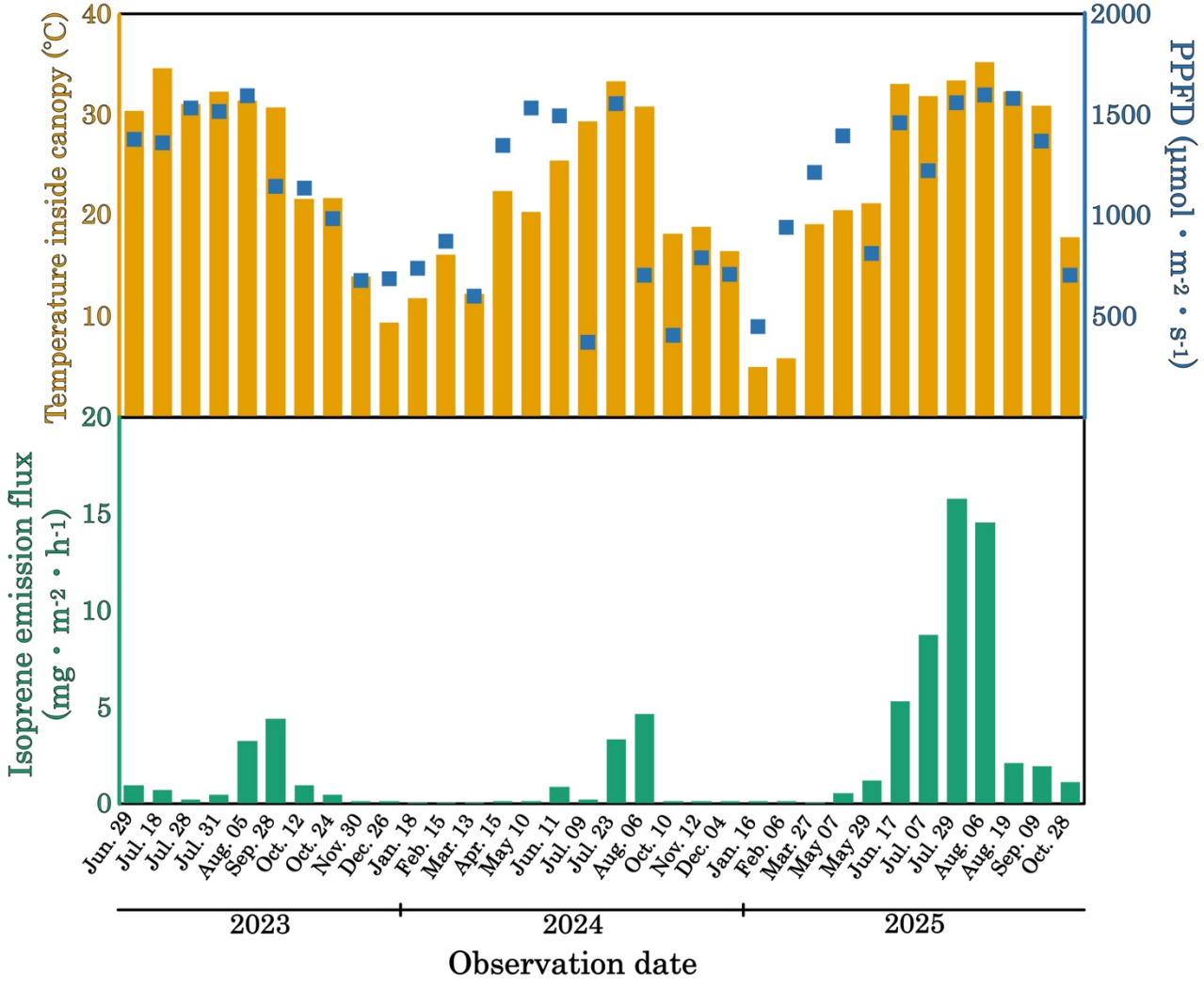

Figure 5: Isoprene emission flux F_{obs} (green bar graph), temperature inside canopy (orange bar graph), and PPFD (red filled square) for observation days from June 2023 to October 2025.

https://doi.org/10.5194/egusphere-2026-2550
Preprint. Discussion started: 26 May 2026

390 **Table 1. Monthly averages of isoprene emission flux, friction velocity, diffusion coefficient, canopy temperature, PPFD, and LAI during the observation period**

Year	Month	Day	F_{obs} (mg・m^{-2}・h^{-1})			u^* (m・s^{-1})			K (m^2・s^{-1})			Canopy Temp. (℃)			PPFD (μmol・m^{-2}・s^{-1})			LAI		
			Ave.	±	Std.	Ave.	±	Std.	Ave.	±	Std.	Ave.	±	Std.	Ave.	±	Std.	Ave.	±	Std.
2023	Jun.	29	0.95	±	0.70	0.46	±	0.05	0.48	±	0.19	30.4	±	1.3	1360	±	639	2.80	±	0.44
	Jul.	18	0.63	±	0.86	0.62	±	0.10	0.58	±	0.13	34.6	±	0.6	1340	±	447	2.67	±	0.52
	Jul.	28	0.21	±	0.85	0.85	±	0.21	0.66	±	0.03	31.1	±	1.0	1513	±	376	3.19	±	0.43
	Jul.	31	0.43	±	0.28	0.83	±	0.22	0.65	±	0.06	32.2	±	0.2	1497	±	403	3.19	±	0.43
	Aug.	5	3.21	±	2.55	1.03	±	0.28	0.74	±	0.09	31.4	±	0.9	1577	±	304	2.94	±	0.58
	Sep.	28	4.22	±	3.95	0.52	±	0.13	0.59	±	0.15	30.7	±	1.7	1127	±	398	2.77	±	0.63
	Oct.	12	0.92	±	0.68	0.47	±	0.17	0.61	±	0.17	21.6	±	0.7	1116	±	469	2.85	±	0.43
	Oct.	24	0.45	±	0.20	0.41	±	0.13	0.57	±	0.16	21.7	±	0.7	967	±	427	3.42	±	0.47
	Nov.	30	0.01	±	0.06	0.62	±	0.25	0.67	±	0.11	13.9	±	1.4	656	±	420	2.23	±	0.63
	Dec.	26	0.00	±	0.03	0.77	±	0.17	0.67	±	0.07	9.4	±	0.7	668	±	326	2.36	±	0.22
2024	Jan.	18	-0.05	±	0.05	0.44	±	0.10	0.66	±	0.14	11.8	±	1.3	717	±	269	1.98	±	0.58
	Feb.	15	-0.02	±	0.03	0.78	±	0.25	0.65	±	0.08	16.1	±	1.3	853	±	341	1.58	±	0.35
	Mar.	13	-0.04	±	0.06	1.40	±	0.15	1.10	±	0.09	12.2	±	0.7	579	±	374	1.02	±	0.21
	Apr.	15	0.08	±	0.06	0.81	±	0.29	0.73	±	0.06	22.5	±	0.9	1329	±	467	1.59	±	0.07
	May	10	0.08	±	0.06	0.81	±	0.29	0.73	±	0.06	20.4	±	0.1	1513	±	379	3.06	±	0.63
	Jun.	11	0.83	±	0.35	0.91	±	0.15	0.66	±	0.05	25.4	±	0.4	1474	±	462	2.25	±	0.46
	Jul.	9	0.25	±	0.40	0.25	±	0.07	0.10	±	0.05	29.3	±	0.5	350	±	243	2.91	±	0.62
	Jul.	23	3.26	±	2.60	0.58	±	0.09	0.51	±	0.07	33.3	±	0.8	1537	±	425	3.16	±	0.79
	Aug.	6	4.53	±	4.60	0.45	±	0.08	0.38	±	0.10	30.8	±	0.9	684	±	284	3.02	±	0.42
	Oct.	10	0.09	±	0.10	0.77	±	0.08	0.46	±	0.09	18.2	±	0.5	385	±	212	2.56	±	0.44
	Nov.	12	0.01	±	0.10	0.59	±	0.14	0.52	±	0.14	18.9	±	0.7	772	±	415	2.52	±	0.50
	Dec.	4	0.00	±	0.00	0.78	±	0.17	0.65	±	0.14	16.5	±	0.5	686	±	363	2.19	±	0.14
2025	Jan.	16	0.00	±	0.00	0.60	±	0.09	0.62	±	0.09	5.0	±	0.8	429	±	106	1.33	±	0.15
	Feb.	6	0.00	±	0.00	0.72	±	0.12	0.70	±	0.07	5.8	±	1.1	922	±	320	1.03	±	0.27
	Mar.	27	0.00	±	0.01	0.63	±	0.13	0.49	±	0.20	19.1	±	1.3	1195	±	422	1.50	±	0.22
	May	7	0.56	±	0.11	1.05	±	0.11	0.72	±	0.10	20.5	±	0.8	1376	±	555	3.02	±	0.82
	May	29	1.14	±	1.07	0.48	±	0.06	0.38	±	0.07	21.2	±	0.6	793	±	388	2.17	±	0.41
	Jun.	17	5.11	±	3.75	0.53	±	0.13	0.51	±	0.10	33.1	±	0.6	1443	±	510	2.83	±	0.75
	Jul.	7	8.43	±	10.85	0.42	±	0.19	0.46	±	0.15	31.9	±	0.4	1205	±	366	3.06	±	0.49
	Jul.	29	15.30	±	9.34	0.56	±	0.17	0.52	±	0.10	33.4	±	0.9	1538	±	417	2.88	±	0.37

https://doi.org/10.5194/egusphere-2026-2550
Preprint. Discussion started: 26 May 2026

Aug.	6	14.02	±	15.33	0.53	±	0.18	0.54	±	0.04	35.3	±	0.3	1579	±	305	2.92	±	0.62
Aug.	19	2.04	±	1.93	0.54	±	0.11	0.54	±	0.03	32.3	±	0.7	1563	±	180	2.92	±	0.62
Sep.	9	1.90	±	3.02	0.49	±	0.16	0.49	±	0.08	30.9	±	0.7	1350	±	293	2.83	±	0.53
Oct.	28	1.04	±	0.60	0.38	±	0.10	0.38	±	0.18	17.9	±	0.9	684	±	343	2.74	±	0.44

The daily average showed clear seasonal variation throughout the observation period. Positive isoprene flux was observed from mid-April during the warm season, with significant fluxes occurring from June to September, and a tendency for fluxes to subside around October. Young leaves have been reported to have lower isoprene emission capacity than mature leaves (Kuzma and Fall, 1993), and a similar trend is observed in *Q. serrata*. Consequently, in April, when young leaves were abundant, relatively low emission flux levels were observed, whereas, from November to March the emission flux levels decreased, showing low values on most days.

High emission flux levels were observed from June to August, and the period averages (medians) were 1.2 (0.6) $mg \cdot m^{-2} \cdot h^{-1}$ in 2023, 2.0 (1.0) $mg \cdot m^{-2} \cdot h^{-1}$ in 2024, and 9.2 (5.2) $mg \cdot m^{-2} \cdot h^{-1}$ in 2025. As shown, 2025 exhibits a tendency toward higher flux levels than other years. As meteorological factors are considered one cause, further explanation will be provided in Section 4.1.

3.3.2 Correlation analysis of isoprene flux and meteorological parameters

The trend pattern of isoprene flux, which begins to rise in spring, peaks in summer, and declines toward the end of autumn, was consistently repeated each year over the approximately 3-year observation period, suggesting that isoprene flux depends on variations in temperature and photosynthetically active radiation (PPFD), as well as the phenology of *Q. serrata*. Next, we analyzed the correlation between isoprene fluxes and these factors. Figure 6 shows a two-dimensional scatter plot based on the entire unaveraged dataset (n=263) for atmospheric temperature within the canopy height (17 m), PPFD, and LAI. As isoprene emissions exhibit exponential or saturated nonlinear relationships with temperature, PPFD, and LAI (Guenther et al., 1993, 2006; Yu et al., 2017), we considered the possibility of nonlinear responses and performed analyses using Spearman's rank correlation coefficient (r_s).

https://doi.org/10.5194/egusphere-2026-2550
Preprint. Discussion started: 26 May 2026

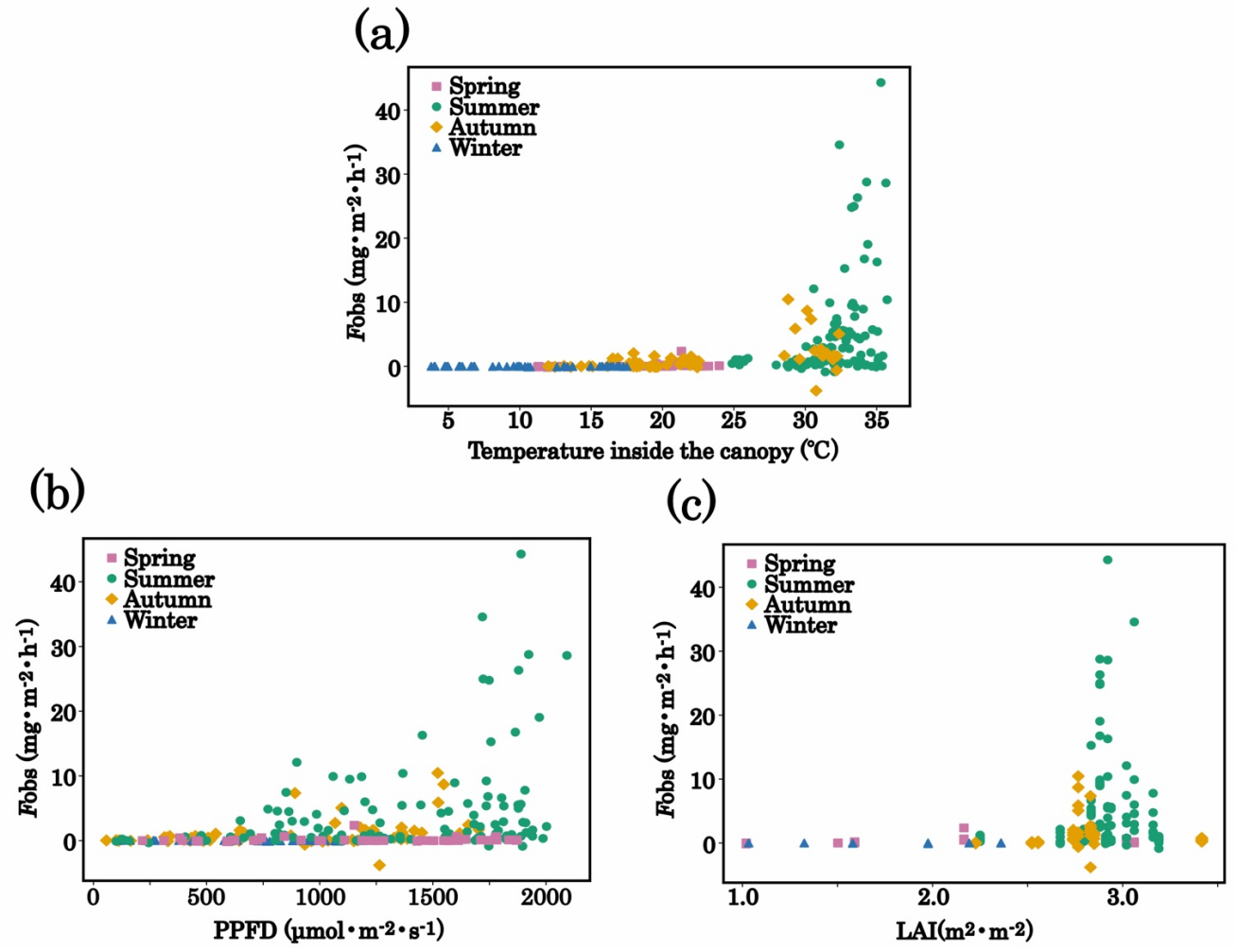

Figure 6: Two-dimensional scatter plots of isoprene emission flux versus various environmental factors: (a) temperature inside the canopy, (b) PPFD, and (c) LAI. Pink squares indicate spring plots, green circles indicate summer plots, orange diamonds indicate autumn plots, and blue triangles indicate winter plots.

The results showed that canopy temperature (r_s=0.71, $p < 0.001$), PPFD (r_s=0.49, $p < 0.001$), and LAI (r_s=0.58, $p < 0.001$) exhibited strong or moderately monotonically increasing relationships with isoprene emissions. Isoprene production is significantly influenced by synthetic substrates (e.g., dimethylallyl diphosphate) generated by photosynthesis within chloroplasts and by isoprene synthase. Photosynthesis is PPFD dependent, and the activity of isoprene synthase is known to be strongly affected by temperature (Rasulov et al., 2010; Chen et al., 2022). Therefore, it is considered that isoprene emissions correlate with temperature and PPFD. According to Rasulov et al. (2010), the pool size of dimethylallyl diphosphate varies with temperature and decreases under high temperature conditions exceeding a threshold, suggesting that elevated temperatures may influence isoprene emission rates. Guenther et al. (1993) observed the relationship between

https://doi.org/10.5194/egusphere-2026-2550
Preprint. Discussion started: 26 May 2026

isoprene emissions and leaf temperature in isoprene emitting trees—Sweetgum, Eucalyptus, Aspen, and Velvet bean. They reported that, depending on the tree species, the emission peak shifted around 35°C, with emission levels decreasing above approximately 40°C. Exceeding the threshold temperature is thought to be associated with the inactivation of the synthetic substrate. The highest temperature recorded during this observation period was 35.7°C, indicating that air temperatures (not leaf temperatures, but considered to be proportional) likely reached levels near the emission peak. Further analysis of isoprene emission, temperature, and PPFD is described in following Section 4.1. LAI is expected to have a positive correlation with isoprene emissions, but once LAI reaches a certain level, emission saturates due to limitations in light availability (Yu et al., 2017).

3.4 Drone-based observation

3.4.1 Horizontal variation in isoprene volume mixing ratio around the flux tower

The average values ± standard deviation of the ratio of isoprene volume mixing ratios obtained at the same time and height (30 m) from tower and drone observations (tower/drone) were plotted as shown in Fig. 7 to evaluate the variability in the horizontal direction. In autumn (horizontal distance between the tower and drone: 15 m), summer (15 m), summer (30 m), and all data, the average values for tower/drone were 0.87, 0.95, 1.32, and 0.99, respectively. Within a 15 m radius of the tower, the horizontal variation was approximately 10%, while at 30 m it was approximately 30%. In Japan, the standard for quality control in the measurement of air pollutants is generally defined as a difference of 30% or less between two or more measurement values obtained independently under the same conditions. As the volume mixing ratio differences due to horizontal variation of isoprene were generally within 30%, it was confirmed that there were no significant deviations.

https://doi.org/10.5194/egusphere-2026-2550
Preprint. Discussion started: 26 May 2026

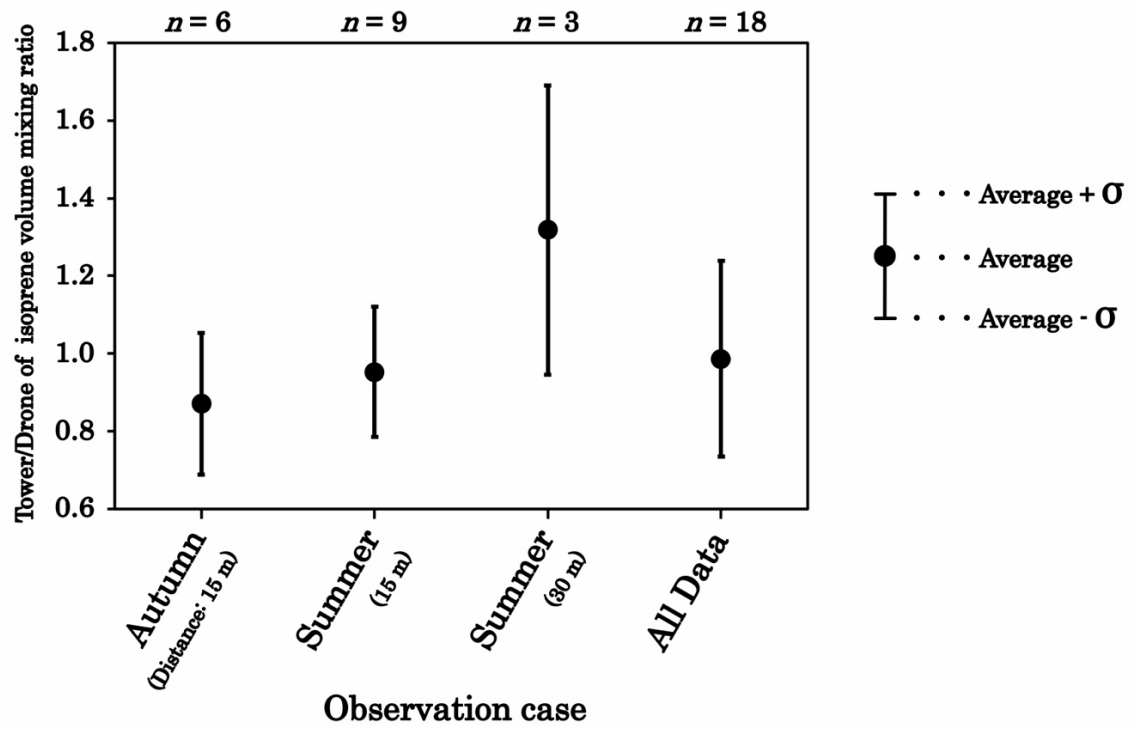

Figure 7: Average and standard deviation of isoprene volume mixing ratios observed at the same height and at the same time by tower and drone on days with different seasons and horizontal distances. The graphs in the figure show, from left to right, autumn (tower-drone distance: 15 m), summer (15 m), summer (30 m), and all data.

The scatter plot between the drone and tower measurements is shown in Fig. 8. The slope of the regression line was 1.05, and the Pearson correlation coefficient was $r = 0.96$ ($p < 0.001$), indicating a very strong positive correlation. This result shows that isoprene measurements taken by the drone are as accurate as those taken at the tower.

https://doi.org/10.5194/egusphere-2026-2550
Preprint. Discussion started: 26 May 2026

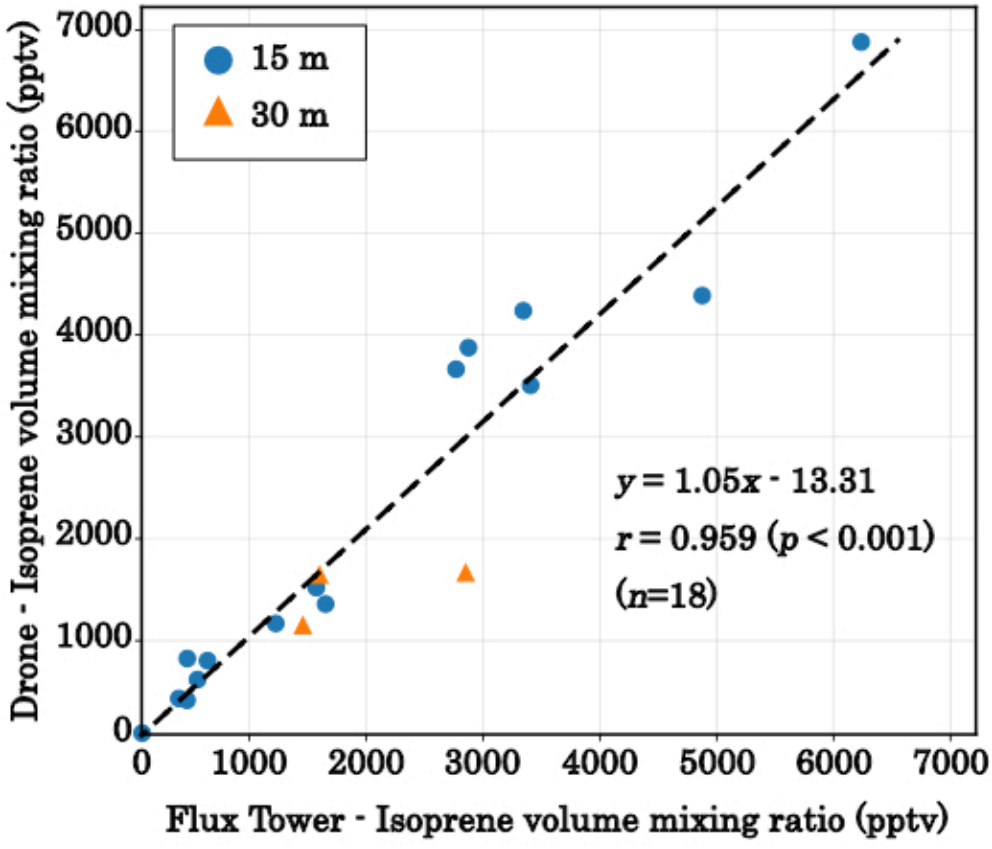

Figure 8: Two-dimensional scatter plots of isoprene volume mixing ratios constructed using drone and tower measurements.

As the distance increased, the volume mixing ratio difference between tower and drone samples grew larger. This difference could be attributed to increased isoprene emission intensity in summer, coupled with the impact of isoprene emission heterogeneity caused by environmental variations such as temperature, light exposure, canopy density, and leaf density. Although drone flight times were limited, spatial variations were confirmed at locations distant from the tower.

3.4.2 Horizontal variation of the isoprene flux

Figure 9 shows the average values ± standard deviation of the isoprene flux ratio (tower/drone) obtained from observations at two different heights using a tower (23–30 m) and a drone (30–40 m). The average flux ratio between the tower and drone for horizontal distance differences of 15 m and 30 m across all data sets was 0.72, 0.98, and 0.85, respectively. Under conditions of a horizontal distance of 30 m, the average flux ratios tended to approach 1 more than under conditions of 15 m. This indicates that the flux due to turbulent vertical transport is complex, and simply increasing the horizontal distance does not necessarily lead to significantly different values. The scatter plot of all isoprene flux data (n = 12) obtained from the tower and drone is shown in Fig. 10. Although a positive correlation was observed between the two

https://doi.org/10.5194/egusphere-2026-2550
Preprint. Discussion started: 26 May 2026

isoprene fluxes, it was not statistically significant ($y = 0.90x + 11.17$, $r = 0.44$, $p = 0.15$). However, when the two data points marked with black circles in the figure, which deviated significantly from the regression line, were excluded, the regression equation became $y = 0.67x + 7.74$, and $r = 0.74$ ($p = 0.015$), indicating a significant positive correlation between the two fluxes.

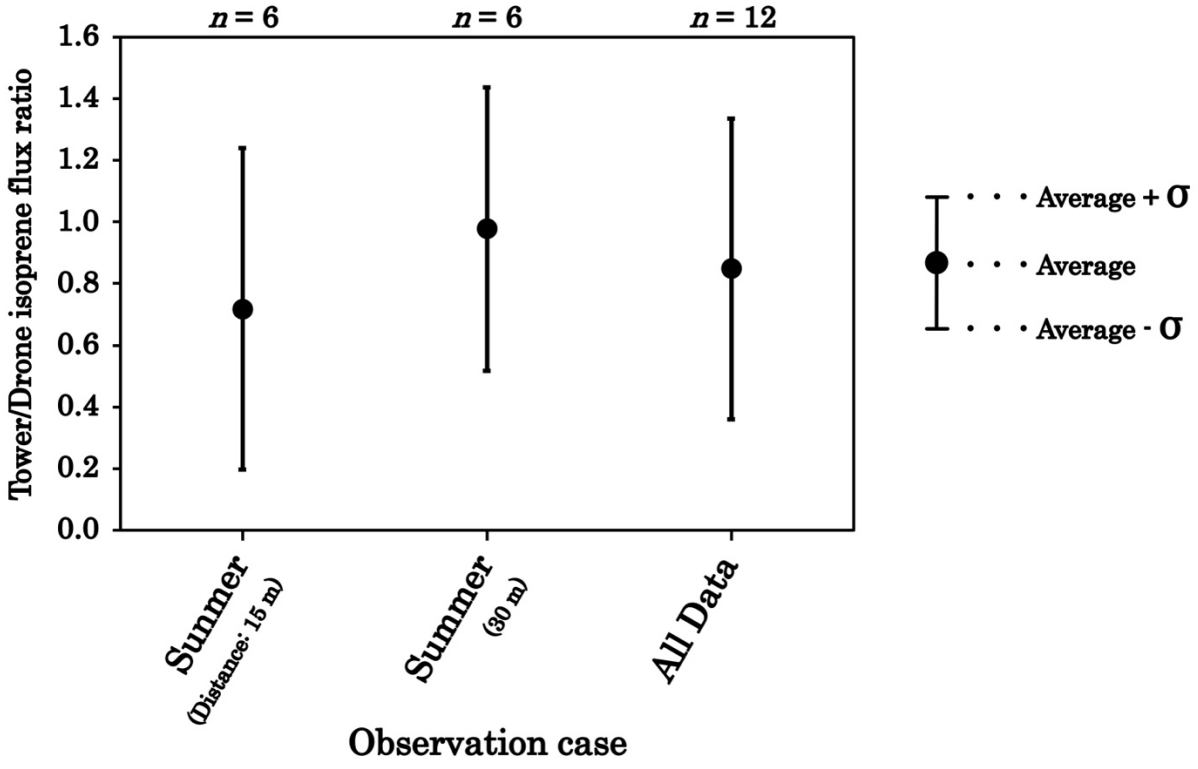

Figure 9: Average and standard deviation of isoprene emission flux ratios observed simultaneously by tower and drone at different horizontal distances during summer. The two heights used for flux calculations based on the aerodynamic gradient method were 23 m and 30 m for the tower, and 30 m and 40 m for the drone. The graphs in the figure show, from left to right: summer (tower-drone distance: 15 m), summer (30 m), and all data.

https://doi.org/10.5194/egusphere-2026-2550
Preprint. Discussion started: 26 May 2026

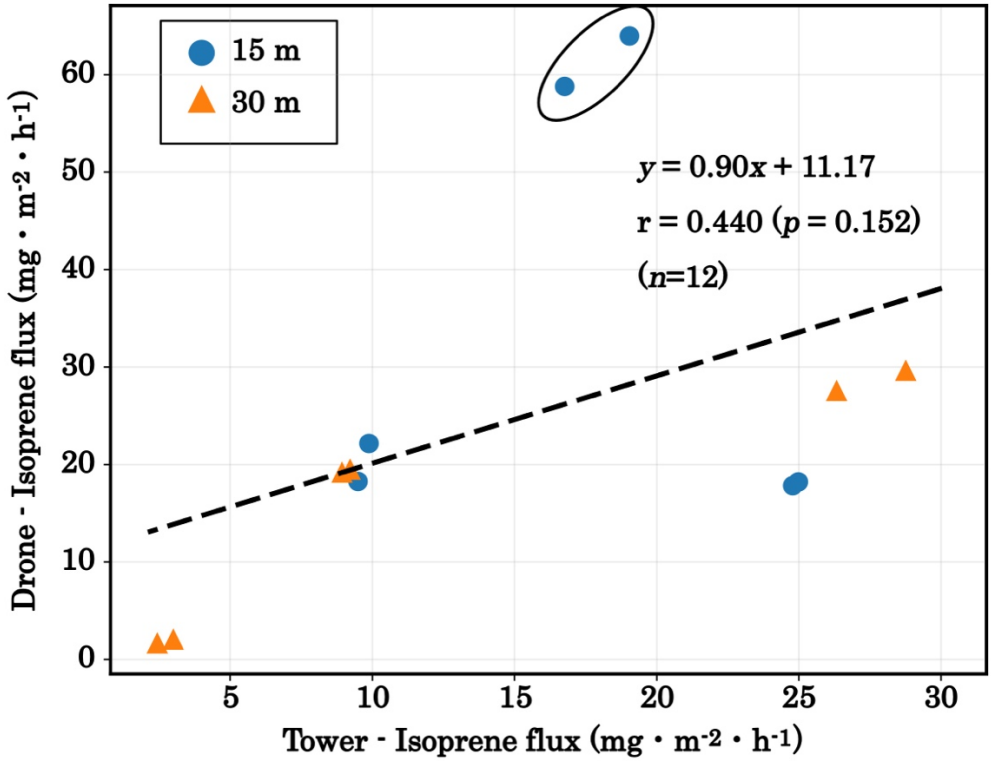

Figure 10: Two-dimensional scatter plot of isoprene fluxes measured by drone and tower. The two data points that deviate significantly from the regression line are marked with black circles.

Although the results regarding the isoprene volume mixing ratio ratio between the drone and the tower, shown in Section 3.4.1, suggest that there are no major issues with the BVOC measurement method used for drones in this study, the following factors were considered to explain the major discrepancies observed in some of the flux ratio data. First, for safety reasons related to drone flight operations, the observation height could not be reduced below 30 m; therefore, the observation height for flux measurements using the drone could not be aligned with that of the tower. Second, while the tower can perform simultaneous sampling at two different heights, it is difficult for drones to carry out similar simultaneous sampling due to payload and equipment constraints. As a result, there is a time lag of approximately 10 min between sampling at 30 and 40 m. Third, since we were unable to install a 3-dimensional ultrasonic anemometer on the drone, we used data from the flux tower. These factors may contribute to the observed differences in flux ratios.

To the best of our knowledge, no known studies have previously estimated flux from drone observations between two heights. This approach was employed in the present study to evaluate the spatial representativeness of flux observations typically conducted on a single tower and the associated observational uncertainties, using actual measurement data. This study represents a novel approach and has yielded interesting results. However, as there is currently a lack of data for further verification, it will be necessary to continue accumulating and verifying measurement data on the spatial variability of fluxes

https://doi.org/10.5194/egusphere-2026-2550
Preprint. Discussion started: 26 May 2026

in the future. Furthermore, as technology advances and improvements are made to drone payload limits and flight times through battery enhancements, it is expected that observations with even lower levels of uncertainty will be possible.

3.5 MEGAN model calculation results

3.5.1 Characteristics and variations of F_{cal} and activity factors

Figure S6 shows the monthly variations in the four activity factors γ_{LAI}, γ_P, γ_T, and γ_{age}, listed alongside F_{cal} for the period from June, 2023, to October, 2025, derived from 10-min values between 10:00 AM and 4:00 PM. The time period was chosen to align with the actual observation period. Note that the period from 11:00 AM on December 1, 2023, to 3:30 PM on February 22, 2024, is treated as missing data due to power outages and equipment maintenance. Additionally, a table presenting monthly statistics for each year is provided as Table S3.

The variation pattern of F_{cal}, which is low during the early spring leaf expansion period, peaking in summer, and gradually decreasing toward the autumn leaf fall period not only replicates the seasonal cycle corresponding to temperature and solar radiation variations, but also reflects the physiological seasonal cycle of *Q. serrata* through LAI and leaf age distribution, showing a tendency consistent with observed values. Focusing on the summer season, which is the primary period for isoprene emission, this study calculates daily mean values limited to the 10:00 AM–4:00 PM time period. As a result, the "daytime peak" component represented by the model is emphasized compared to full-day averages, and the impact of high emission flux days is significantly amplified. Seasonal averages (median values) were 7.4 (6.1), 7.3 (5.7), and 8.5 (7.6) $mg \cdot m^{-2} \cdot h^{-1}$ for 2023, 2024, and 2025, respectively. Over the three-year period, the model estimates showed the highest daily average flux in the summer of 2025, which is also consistent with the observed results.

γ_{LAI} begins to rise gradually around early spring in March, and from May to October, it generally remains saturated at around 0.8–0.9. γ_P maintains a base level of around 0.4–0.5 even during winter, but rises to approximately 0.7–0.9 between June and August. γ_T exhibits large variations, being very small at around 0.1 during winter, while reaching an average value of approximately 1.2–1.4 during July–August, suggesting it contributes significantly to the annual cycle F_{cal}. γ_{age} begins to rise around spring, remains high at around 0.9 from June through September, declines slightly from October through November, and drops to 0 during the leaf-fall season.

To quantitatively evaluate the relationship between F_{cal} and γ_P, γ_T, Spearman's rank correlation coefficient (r_s) was calculated from 10-min data collected during the period from May to October when isoprene emission levels are relatively high. As a result, the correlation coefficients were γ_P (r_s=0.86, p<0.001) and γ_T (r_s=0.89, p<0.001), indicating a very high positive correlation. This is consistent with physiological findings that isoprene emissions from leaves strongly depend on photosynthetic activity and temperature, supporting that MEGAN's algorithm for light and temperature response scheme in FM Tama appropriately captures the main temporal variation factors of the emission.

3.5.2 Comparison of F_{obs} and F_{cal}

https://doi.org/10.5194/egusphere-2026-2550
Preprint. Discussion started: 26 May 2026

The comparison was performed using F_{obs} and F_{cal} for the period from May to October, when isoprene emission fluxes are dominant, analyzing data from the observed day and time. The analysis period covered 24 d observation. The data comparison diagram is shown in Fig. 11, and statistical data, MEB and RMSE are summarized in Table 2.

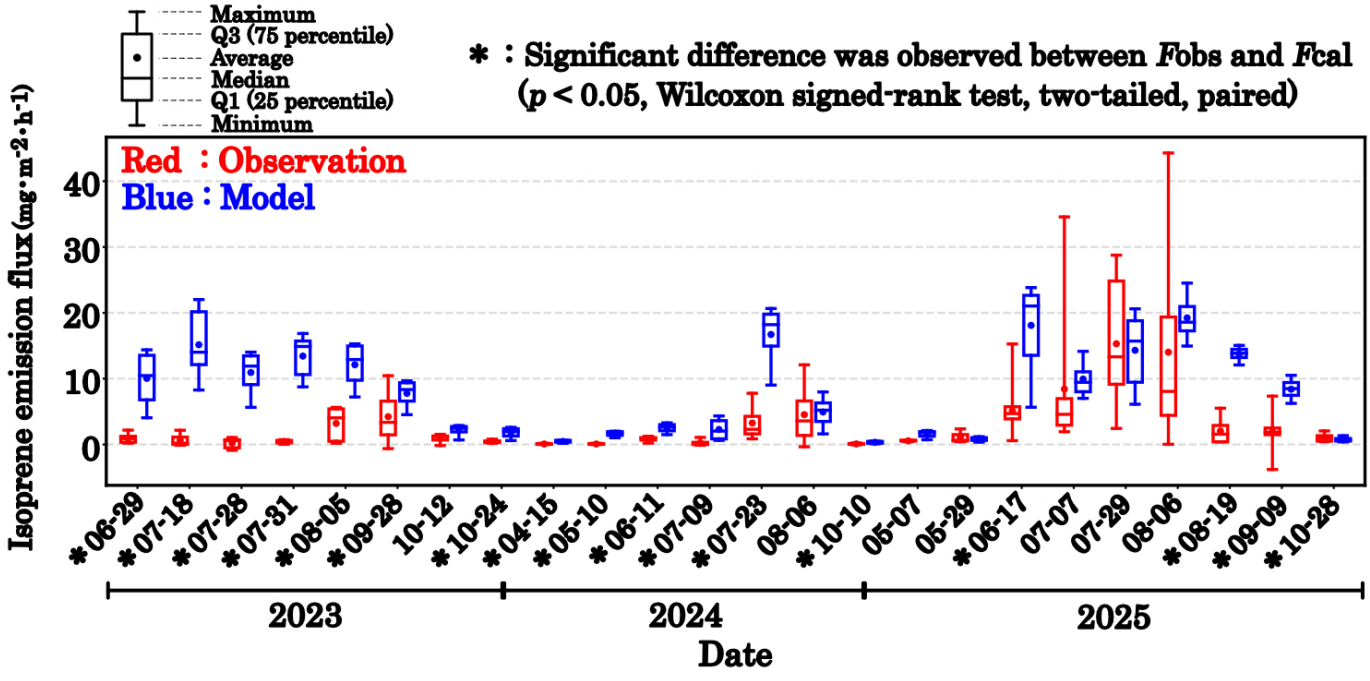

Figure 11: Comparison of boxplots and average values for F_{obs} and F_{cal} on observation days during the period from May to October, when isoprene emissions are significant.

Table 2. Number of data points (n) used for comparative evaluation of F_{obs} and F_{cal} across all spring, summer, and autumn data, along with calculated results for mean error bias (MEB) and root mean square error (RMSE).

	n	MEB[1)]	RMSE[1)]
Spring	22	0.80	1.11
Summer	112	7.20	10.54
Autumn	45	2.16	3.76
Overall	179	5.15	8.56

1) unit: $mg \cdot m^{-2} \cdot h^{-1}$

As the average for the entire period (n=179), MEB=+5.15 $mg \cdot m^{-2} \cdot h^{-1}$ and RMSE=8.56 $mg \cdot m^{-2} \cdot h^{-1}$. As MEB is positive, MEGAN showed a tendency to estimate flux higher than the observed values (overestimation). Given that the RMSE is also

https://doi.org/10.5194/egusphere-2026-2550
Preprint. Discussion started: 26 May 2026

relatively large, when correcting MEGAN to match observed values, it is highly likely that unaccounted variability factors are influencing the results, which cannot be explained by a simple fixed subtraction.

When decomposed by season, MEB and RMSE were +0.80 $mg \cdot m^{-2} \cdot h^{-1}$ and 1.11 $mg \cdot m^{-2} \cdot h^{-1}$ for spring (n=22), +7.20 $mg \cdot m^{-2} \cdot h^{-1}$ and 10.54 $mg \cdot m^{-2} \cdot h^{-1}$ for summer (n=112), and +2.16 $mg \cdot m^{-2} \cdot h^{-1}$ and 3.76 $mg \cdot m^{-2} \cdot h^{-1}$ for autumn (n=45), with summer showing particularly significant errors. The fact that trends differ by season is an important finding obtained through long-term observation in this study. Spring shows smaller MEB and RMSE, with MEGAN and observations relatively well-matched. Summer, however, exhibits the largest MEB and RMSE, featuring not only average overestimation but also likely containing discrepancies in the reproducibility of diurnal variations. Autumn shows reduced errors compared to summer; however, a positive bias persists. This seasonal difference is consistent with the strong light and temperature dependence of isoprene emissions. During summer, the effects of γ_T and γ_P become particularly pronounced, making it likely that discrepancies between the representativeness of the input and the actual foliar environment within the canopy are amplified as errors.

For each observation day, we evaluated the significance of daily distribution differences using the Wilcoxon signed-rank test (two-tailed, paired) with paired F_{obs} and F_{cal} data collected at the same time. The 22 d for which the number of daily pairs met the general threshold (5 or more) were included in the test. The remaining two days (May 7, 2025, and May 29, 2025) were excluded from the test because they had only 3 pairs. The test results showed significant differences (p<0.05) on 17 of the 22 d. On 16 of those days, F_{cal} tended to overestimate.

Seasonal linear regression using time-synchronized pair data and daily averages ($F_{cal} = a \times F_{obs} + b$) is shown in Fig. 12. For all seasons, the intercept was positive, suggesting a tendency for MEGAN to assign a certain level of flux even under low observation conditions. Notably, the summer intercept was large, indicating a tendency toward significant overestimation in the low F_{obs} range. Conversely, the slope fell below 1 in both summer and autumn, suggesting a relatively sluggish model response to increasing observations and potentially insufficient tracking of high emission events.

https://doi.org/10.5194/egusphere-2026-2550
Preprint. Discussion started: 26 May 2026

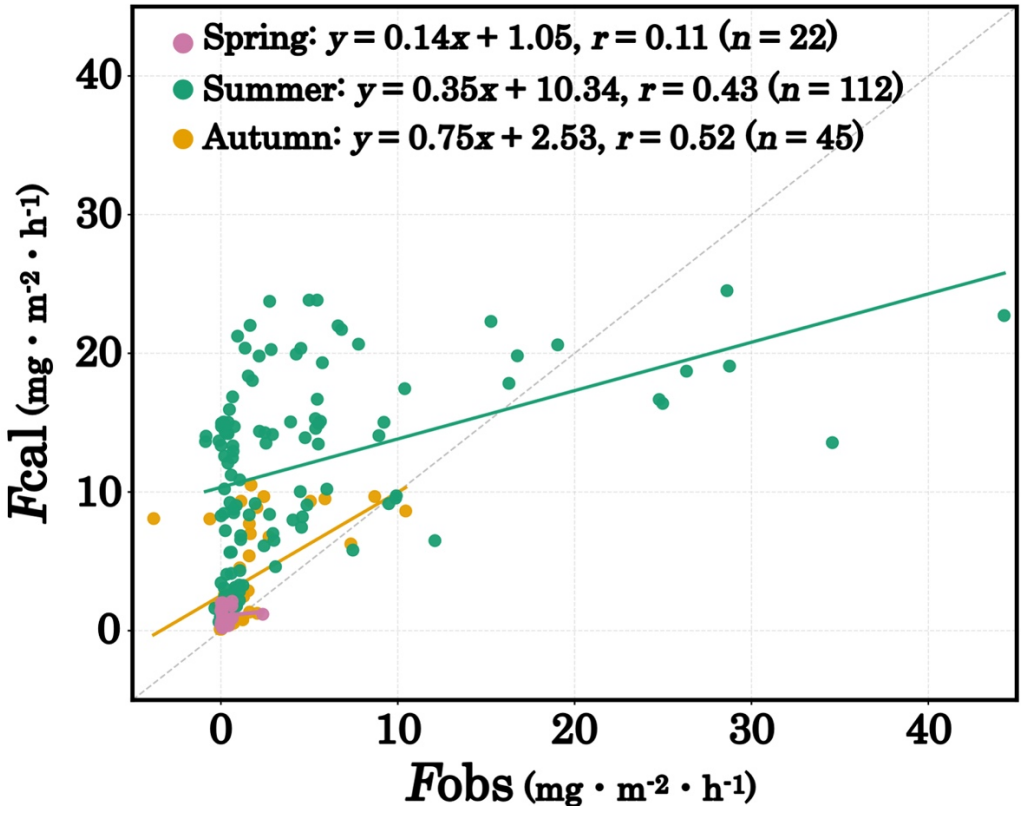

Figure 12: Scatter plot of F_{obs} and F_{cal}. Pink circles indicate spring data, green circles indicate summer data, and orange circles indicate autumn data. The upper left shows the regression equations obtained by least squares fitting from the seasonal data.

4. Discussion

4.1. High isoprene emissions in summer 2025

The summer of 2025 showed significantly higher isoprene emissions compared to the summers of 2023 and 2024, both in F_{obs} and F_{cal}. According to the Japan Meteorological Agency (2025), the 2025 rainy season ended earlier than usual, and in June and July, record-high temperatures were observed across northern, eastern, and western Japan, with the summer average temperature deviation reaching +2.36°C, significantly surpassing past records. This was due to the Tibetan anticyclone extending over Japan as a result of the upper-level westerlies flowing northward from June onward, influenced by the early and active development of the Asian monsoon. Furthermore, the expansion of the Pacific anticyclone coincided with this, bringing clear skies and rising temperatures. Consequently, the cumulative number of locations recording daily maximum temperatures of 40°C or higher also set a new record.

The average canopy temperatures at the FM Tama during the summers of 2023, 2024, and 2025 were 25.55°C, 25.81°C, and 26.32°C, respectively. When the average temperature at the time of observation was calculated, the figures for 2023, 2024, and 2025 were 31.96°C, 29.34°C, and 33.19°C, respectively, with 2025 recording the highest temperature across the 3

https://doi.org/10.5194/egusphere-2026-2550
Preprint. Discussion started: 26 May 2026

years. Meanwhile, the average PPFD, another environmental factor contributing to isoprene flux intensity, during the summer observation period was 1,161, 1,095, and 1,021 μmol·m^{-2}·s^{-1} in 2023, 2024, and 2025, respectively. Unlike temperature, the average PPFD was lowest in 2025, and it is believed that PPFD is not strongly correlated with the high increase in flux expected in 2025. Furthermore, there were no significant differences in wind direction and speed during the summer months over the 3-year period.

The average (rate of change) isoprene emissions in the summer of 2025 increased by +7.2 (360%) mg·m^{-2}·h^{-1} for F_{obs} and +1.2 (16%) mg·m^{-2}·h^{-1} for F_{cal} compared to the previous year. Kramshøj et al. (2016) conducted a field experiment in the dry shrub tundra of West Greenland, where *Empetrum hermaphroditum* and the isoprene-emitting species *Salix glauca* co-dominate. Using the enclosure method, which involves enclosing the entire ecosystem plot (33 × 33 cm) comprising the vegetation and the underlying soil, the authors reported that when the temperature inside the enclosure was increased by an average of 3.1°C, BVOC emissions from the entire ecosystem increased by 260% compared with those in the control area. Although the tundra region differs in terms of climate and vegetation and, therefore, cannot be simply compared with Japan, which has a humid subtropical climate, the average temperature on the observation day in 2025 was approximately 1.23°C and 3.85°C higher than that in 2023 and 2024, respectively. Thus, it is possible that fluxes increased alongside temperature in 2025.

Figure 13 shows a scatter plot of summer isoprene flux and temperature inside canopy, plotted for each year. Even under the same high-temperature conditions, the flux varied significantly from year to year. The scatter plot shows that high fluxes were frequently observed in 2025 (approximately 32–35°C), and higher emissions were confirmed within this temperature range compared with those in 2023 and 2024.

https://doi.org/10.5194/egusphere-2026-2550
Preprint. Discussion started: 26 May 2026

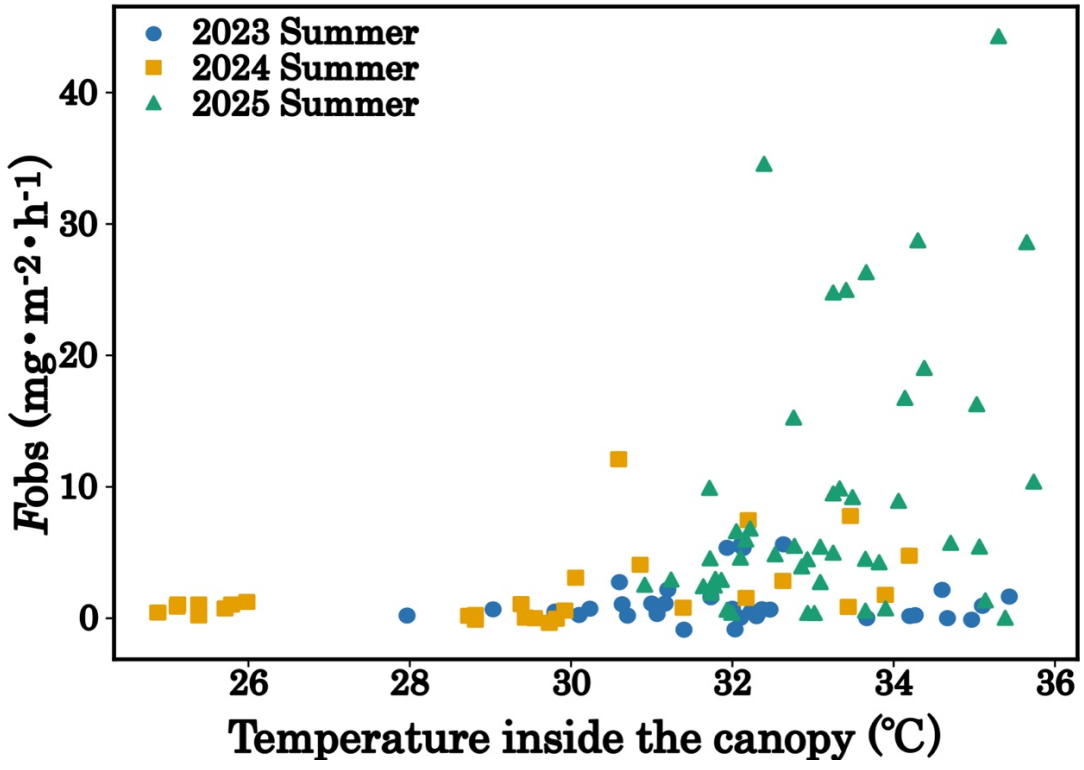

Figure 13: Two-dimensional scatter plot of isoprene emission flux and temperature inside the canopy for each summer. 2023 is indicated by blue circles, 2024 by orange squares, and 2025 by green triangles.

The lower increase in F_{cal} compared to F_{obs} is thought to be due to the relatively sluggish response of MEGAN to high flux levels, as shown in Section 3.5.2, which results in insufficient tracking of high-emission events. In any case, we believe that the increase in isoprene emissions in 2025 was due to the unusually early end of the rainy season and rising temperatures, suggesting the influence of global warming and climate change. The ability to detect a significant upward trend in isoprene emissions under the climatic conditions in Japan in 2025, a year marked by record-breaking temperature rises due to the progression of global warming, was made possible by conducting interannual comparisons based on long-term observations.

Megaritis et al. (2013) predicted that a 2.5°C rise in temperature in Northern Europe would lead to an increase in BVOC emissions, resulting in a 20% increase in summer biogenic SOA. Moreover Churkina et al. (2017) estimated that increased BVOC emissions during heatwave events in the Berlin-Brandenburg metropolitan area of Germany contribute up to 60% to O_3 formation, indicating that the impact of BVOC increases due to high temperatures on the atmospheric environment is significant. Furthermore, Wang et al. (2024) warn that during heat waves, plants not only increase the production of O_3 precursors but also close their stomata, thereby reducing the dry deposition of O_3 (making it harder to remove); consequently, the increasing frequency of heat waves poses a major challenge for air pollution control.

https://doi.org/10.5194/egusphere-2026-2550
Preprint. Discussion started: 26 May 2026

Due to global warming, high temperatures have persisted, and there are concerns that this trend will continue. Numerous observational and modeling studies indicate that temperature significantly contributes to BVOC emissions and predict increased isoprene emissions due to global warming (Okumura et al., 2008; Emmerson et al., 2020; Hata et al., 2023; Kramshøj et al., 2016). It is important to continue conducting thorough monitoring of BVOC emissions in response to changes in the global environment.

4.2. Analysis of isoprene emission flux with temperature and PPFD

Observations in this study confirmed that temperature and PPFD significantly influence isoprene emission flux, consistent with previous research (Guenther et al., 1993; Bao et al., 2008). To examine these factors in combination, a 3-dimensional scatter plot of F_{obs}, temperature inside the canopy, and PPFD was created (Fig. S7). Under high temperature and high PPFD conditions, F_{obs} tend to be high, but cases with low flux are also observed. This indicates that while temperature and light are the primary drivers, other factors may also govern flux variations, at least during certain periods and under specific conditions.

To analyze the factors involved, we first calculated the 75th percentile (Q3) for both temperature and PPFD from the entire observation dataset (n=263). We then extracted data points simultaneously satisfying temperature ≥ Q3 (approximately 32°C) and PPFD ≥ Q3 (approximately 1571 μmol·m^{-2}·s^{-1}). The F_{obs} distribution of this subset (n=37, of which 36 were summer and 1 was autumn) was classified as follows. L-F_{obs} denotes the group below the 25th percentile (approximately 1.5 mg·m^{-2}·h^{-1}, n=10), and corresponds to the data points marked with black circles in Fig. S7. Although we were unable to identify a clear cause for the occurrence of L-F_{obs}, factors unrelated to meteorological conditions, such as the spatial structure of the source distribution and the uneven distribution of unidentified shrubs and herbaceous plants, may play a crucial role.

4.3. Considerations on discrepancies between observed values and MEGAN calculations

MEGAN overestimated observed values during spring, summer, and autumn, where isoprene emissions were detected. Particularly during summer, when BVOC emissions are high and contribute to O_3 and SOA formation, reducing the discrepancy with observed values is crucial for developing atmospheric environmental countermeasures and strategies and constructing future predictions.

Guenther et al. (2012) estimated the uncertainty in isoprene emission from MEGAN to be approximately on a factor of two. Emmerson et al. (2016) found that MEGAN overestimated isoprene flux by a factor of three compared to observations obtained using PTR-MS and eddy covariance flux measurements for eucalypt species known as high isoprene emitters in southeastern Australia. Given that uncertainties differing by several factors or orders of magnitude would inevitably lead to significant discrepancies from reality, both observational data and model calculations inherently involve uncertainty, making perfect agreement impossible. However, identifying the causes of these discrepancies and taking steps to address them hold academic importance.

https://doi.org/10.5194/egusphere-2026-2550
Preprint. Discussion started: 26 May 2026

Regarding spatial uncertainty in tower observations, we verified horizontal variation in both isoprene volume mixing ratio and flux. For horizontal variation of isoprene volume mixing ratio with relatively similar sampling conditions, volume mixing ratio variations within a 15–30 m radius of the tower were found to be within 30%. Although the uncertainty in the flux was expected to be higher due to differences in measurement height relative to that of the tower caused by safety considerations for the drone, as well as limitations on micro-meteorological factors on the drone side, it remained within 30%. These results indicate that spatial uncertainty of this magnitude is to be expected.

The basal emission rate (ε) assigned in MEGAN based on plant functional type (PFT) serves as the foundation for model estimation, but Langford et al. (2017) raised concerns that it was calculated based on a very limited number of leaf-level observations, resulting in extremely high uncertainty. Tani et al. (2024) summarized past leaf-level measurement data and highlighted that differences in measurement methods can cause variation in ε even within the same tree species. Furthermore, Geron et al. (2000) studied the seasonal variability of ε in multiple leaves of white oak (*Quercus alba L.*) under standard conditions of the G93 model, reporting that it fluctuated significantly throughout the summer and also exhibited diurnal variation of approximately two-fold. Additionally, Okumura et al. (2008) conducted field observations using the leaf cuvette method on mature *Q. serrata* in the forests of Yamashiro, Kyoto. They found that the ε at the leaf level for sunlit leaves was 42.9 $nmol \cdot m^{-2} \cdot s^{-1}$, while shaded leaves showed a rate of 20.5 $nmol \cdot m^{-2} \cdot s^{-1}$. Therefore, ε is considered to possess an extremely complex nature. In MEGAN, changes in emission due to seasonally varying weather, leaf phenology, and environmental conditions are structured to be scaled by γ. However, based on these prior studies, it may be necessary to consider factors such as environmental conditions, region, and seasonality for ε as well, rather than treating it as a fixed value throughout the year.

As confirmed in this study, because the activity factors γ exhibit a particularly pronounced positive correlation response with emission flux, especially with respect to γ_T, they may also significantly contribute to the uncertainty. Emmerson et al. (2020) measured isoprene using the leaf cuvette method across four Eucalyptus species at temperatures ranging from 293–328 K in 5 K increments, reporting that the temperature-dependent peak occurs at higher temperatures than in the original MEGAN study. DiMaria et al. (2023) argue that developing γ_T parameterizations optimized for each ecosystem is necessary to accurately model the temperature sensitivity of isoprene emission. Previous studies on the emission characteristics of BVOC under high-temperature conditions did not consider evaluating sensitivity of native plant species to γ_T due to advancing climate warming. Furthermore, in calculating activity factors γ, a significant amount of empirical data established during the MEGAN development process has been utilized. It would be worthwhile to verify whether these values truly represent the optimal values for each region.

5. Conclusion

The key features of this study are the long-term, multi-height BVOC observations using a flux tower and isoprene flux measurements using the aerodynamic gradient method (AGM) in a research forest (a mixed forest dominated by *Quercus serrata*) in the suburbs of Tokyo, which has a humid subtropical climate. Additionally, we evaluated the spatial variability of

https://doi.org/10.5194/egusphere-2026-2550
Preprint. Discussion started: 26 May 2026

isoprene through integrated observations with drone and assessed the reproducibility of MEGAN. The observation period lasted approximately two and a half years, from June 2023 to October 2025. Multi-height BVOC observations were conducted at four heights: 30 m, 23 m, 17 m, and 3 m above ground level.

Observations from the tower revealed that during the cold season (November–April), each BVOC component was present at low volume mixing ratios with small vertical differences. In contrast, during the warm season (May–October), isoprene volume mixing ratios surged dramatically, accounting for over 90% of the BVOC composition in July and August. Vertically, isoprene volume mixing ratios peaked at 17 m, corresponding to the canopy layer. During the warm season, the volume mixing ratio difference between the canopy layer and the above-canopy layer increased, forming a distinct vertical gradient. This confirmed that the primary source of isoprene is within the canopy, and that emitted isoprene is transported upward by turbulent transport. In contrast, monoterpenes generally remained at low volume mixing ratios throughout the year, and the vertical gradient was not distinct. Long-term data confirmed that isoprene is the dominant BVOC at this site.

Isoprene emission flux calculated by AGM ranged from −0.05 to 15.30 $mg \cdot m^{-2} \cdot h^{-1}$ on a daily average basis, with a seasonal pattern showing a peak during summer. The seasonal average (median) for summer (June–August) was notably higher in 2025 at 9.2 (5.2) $mg \cdot m^{-2} \cdot h^{-1}$, compared to 1.2 (0.6) $mg \cdot m^{-2} \cdot h^{-1}$ in 2023 and 2.0 (1.0) $mg \cdot m^{-2} \cdot h^{-1}$ in 2024. The high emission flux in 2025 is considered to be due to the historically high temperatures recorded that year. This result suggests that annual isoprene emission may increase as temperatures rise with future global warming. The relationship between isoprene flux and environmental factors revealed a significant positive relationship with temperature inside the canopy, PPFD, and LAI, clearly demonstrating that emissions are controlled by temperature, sunlight, and leaf area (phenology).

Regarding spatial variability assessment through integrated tower and drone observations, horizontal heterogeneity near the tower was quantified. The volume mixing ratio of tower/drone at the same height (30 m) and time showed an average of approximately 0.87–0.95 at a horizontal distance of 15 m. This can be summarized as approximately 10% variation at the 15 m scale. However, at a distance of 30 m, the average was 1.32, indicating that the heterogeneity expanded to approximately 30% at the 30 m scale. This heterogeneity was more pronounced during the warm season, suggesting that under conditions of active isoprene emissions, differences in tree species composition, microtopography, and canopy structure are reflected in volume mixing ratio patterns. Moreover, to the best of our knowledge, this study represents the first observational attempt to estimate isoprene flux between two heights using drone-based measurements. The estimated flux agreed with the tower-based flux within approximately 30% at a horizontal distance of 30 m.

Comparing flux tower observations with MEGAN revealed a clear tendency for the model to consistently overestimate observed flux values. Simultaneous comparisons from May to October (n=179) yielded MEB=+5.15 and RMSE=8.56 $mg \cdot m^{-2} \cdot h^{-1}$. When examined seasonally, the errors followed the order summer > autumn > spring. During summer, MEB=+7.20 and RMSE=10.54, with overestimation becoming particularly pronounced during periods of high emission conditions. This divergence suggests that basal emission rate (ε), temperature response (γ_T), light response (γ_P), leaf area

https://doi.org/10.5194/egusphere-2026-2550
Preprint. Discussion started: 26 May 2026

(γ_{LAI}) and other factors may not sufficiently match site-specific conditions. Furthermore, it indicates that uncertainties stemming from spatial variability on the observational side are also present.

To more accurately characterize the impacts of BVOC on global environmental systems such as air quality, climate, and the carbon cycle under conditions of advanced global warming, further observations and quantitative analyses of BVOC emissions are necessary. Future research priorities for this work include re-evaluating site-specific ε and activity factors γ, as well as verifying alternative estimation models. Furthermore, the incorporation of multi-point aerial observations using drone has yielded promising results. Progress in observationally constraining horizontal and vertical heterogeneity is expected to contribute to improving the reliability of evaluating canopy-scale spatial variability of BVOCs and reducing uncertainties in regional emission inventories and air quality predictions.

Code and data availability

The BVOC data observed in this study and the computational data from the MEGAN model are available from the JPCOAR Cloud site (https://cess.repo.nii.ac.jp/records/2000003), a repository constructed and operated by the Japan Consortium for Open Access Repository (Open Access Repository Promotion Association).

Author contributions

YI: Conceptualization, Data curation, Formal analysis, Funding acquisition, Investigation, Methodology, Project administration, Software, Validation, Visualization, Writing – original draft. KY: Investigation, Writing – review and editing. SY: Conceptualization, Funding acquisition, Methodology, Writing – review and editing. KT: Resources, Writing – review and editing. AS: Supervision, Writing – review and editing. KM: Resources, Supervision, Writing – review and editing. TO: Conceptualization, Funding acquisition, Methodology, Supervision, Writing – review and editing.

Competing interests

The contact author has declared that none of the authors has any competing interests.

Disclaimer

Publisher's note: Copernicus Publications remains neutral with regard to jurisdictional claims made in the text, published maps, institutional affiliations, or any other geographical representation in this paper. The authors bear the ultimate responsibility for providing appropriate place names. Views expressed in the text are those of the authors and do not necessarily reflect the views of the publisher.

Acknowledgements

Drone flight was assisted by Mr. Yuji Yamamoto and Mr. Hiroto Watanabe of Green Blue Co., Ltd. We would like to express our gratitude to them.

https://doi.org/10.5194/egusphere-2026-2550
Preprint. Discussion started: 26 May 2026

Financial support

This work was supported by Japan Society for the Promotion of Science KAKENHI (grant number 23K11413).

References

Altamira-Colado, E., Cuevas-González, D., Reyna, M. A., García-Vázquez, J. P., Avitia, R. L., and Osornio-Vargas, A. R.: Drone-assisted particulate matter measurement in air monitoring: A patent review, Atmosphere, 15, 515, https://doi.org/10.3390/atmos15050515, 2024.

Atkinson, R., and Arey, J.: Atmospheric degradation of volatile organic compounds, Chem. Rev., 103, 4605–4638. https://doi.org/10.1021/cr0206420, 2003.

Bai, J., Guenther, A. B., Turnipseed, A., Duhl, T., Yu, S., and Wang B.: Seasonal variations in whole-ecosystem BVOC emissions from a subtropical bamboo plantation in China, Atmos. Environ., 124, 12–21, https://doi.org/10.1016/j.atmosenv.2015.11.008, 2016.

Bai, J., Wu, Z., Yang, C., and Guenther, A.: Seasonal variations in whole–ecosystem BVOC emissions and ozone fluxes from a tropical rubber tree plantation in China, Atmos. Environ., 351, 121182, https://doi.org/10.1016/j.atmosenv.2025.121182, 2025.

Baker, B., Bai, J. H., Johnson, C., Cai, Z. T., Li, Q. J., Wang, Y. F., Guenther, A., Greenberg, J., Klinger L., Geron, C., Rasmussen, R.: Wet and dry season ecosystem level fluxes of isoprene and monoterpenes from a southeast Asian secondary forest and rubber tree plantation, Atmos. Environ., 39, 381–390, https://doi.org/10.1016/j.atmosenv.2004.07.033, 2005.

Bao, H., Kondo, A., Kaga, A., Tada, M., Sakaguti, K., Inoue, Y., Shimoda, Y., Narumi, D., and Machimura, T. (2008). Biogenic volatile organic compound emission potential of forests and paddy fields in the Kinki region of Japan, Environ. Res., 106, 156–169, https://doi.org/10.1016/j.envres.2007.09.009, 2008.

Bouvier-Brown, N. C., Schade, G. W., Misson, L., Lee, A., Mckay, M., and Goldstein, A. H.: Contributions of biogenic volatile organic compounds to net ecosystem carbon flux in a ponderosa pine plantation, Atmos. Environ., 60, 527–533, https://doi.org/10.1016/j.atmosenv.2012.06.070, 2012.

Celedon, J. M., and Bohlmann, J.: Oleoresin defenses in conifers: chemical diversity, terpene synthases and limitations of oleoresin defense under climate change, New Phytol., 224, 1444–1463, https://doi.org/10.1111/nph.15984, 2019.

Chatani, S., Matsunaga, S. N., and Nakatsuka, S.: Estimate of biogenic VOC emissions in Japan and their effects on photochemical formation of ambient ozone and secondary organic aerosol, Atmos. Environ., 120, 38–50, https://doi.org/10.1016/j.atmosenv.2015.08.086, 2015.

Chatani, S., Kokubu, Y., Takahashi, K., and Hoshi, J.: Validation of emission inventories and air quality simulations based on concentrations of individual VOC species measured in Tokyo, J. Jpn. Soc. Atmos. Environ., 57, 35–52, https://doi.org/10.11298/taiki.57.35, 2022.

https://doi.org/10.5194/egusphere-2026-2550
Preprint. Discussion started: 26 May 2026

Chen, Y.-J., Huang, Y.-L., Chen, Y.-H., Chang, S.-T., and Yeh, T.-F.: Biogenic volatile organic compounds and protein expressions of *Chamaecyparis formosensis* and *Chamaecyparis obtusa* var. formosana leaves under different light intensities and temperatures, Plants, 11, 1535. https://doi.org/10.3390/plants11121535, 2022.

Churkina, G., Kuik, F., Bonn, B., Lauer, A., Grote, R., Tomiak, K., and Butler, T. M.: Effect of VOC emissions from vegetation on air quality in Berlin during a heatwave, Environ. Sci. Technol., 51, 6120–6130, https://doi.org/10.1021/acs.est.6b06514, 2017.

DiMaria, C. A., Jones, D. B. A., Worden, H., Bloom, A. A., Bowman, K., Stavrakou, T., Miyazaki, K., Worden, J., Guenther, A., Sarkar, C., Seco, R., Park, J-H., Tota, J., Alves, E. G., and Ferracci, V.: Optimizing the isoprene emission model MEGAN with satellite and ground-based observational constraints, J. Geophys. Res., 128, e2022JD037822, https://doi.org/10.1029/2022JD037822, 2023.

Dumont, C., Verreyken, B. W. D., Schoon, N., Bergmans, B., Heinesch, B., and Amelynck, C.: Multi-year observations of BVOCs and ozone: concentrations and fluxes measured above and below the canopy in a mixed temperate forest, Earth Syst. Sci. Data, 18, 617-654, https://doi.org/10.5194/essd-18-617-2026, 2026.

Emmerson, K. M., Galbally, I. E., Guenther, A. B., Paton-Walsh, C., Guerette, E.-A., Cope, M. E., Keywood, M. D., Lawson, S. J., Molloy, S. B., Dunne, E., Thatcher, M., Karl, T., and Maleknia, S. D.: Current estimates of biogenic emissions from eucalypts uncertain for southeast Australia, Atmos. Chem. Phys., 16, 6997–7011, https://doi.org/10.5194/acp-16-6997-2016, 2016.

Emmerson, K. M., Possell, M., Aspinwall, M. J., Pfautsch, S., and Tjoelker, M. G.: Temperature response measurements from eucalypts give insight into the impact of Australian isoprene emissions on air quality in 2050, Atmos. Chem. Phys., 20, 6193-6206, https://doi.org/10.5194/acp-20-6193-2020, 2020.

EPA: https://www.epa.gov/sites/default/files/2019-12/documents/to-15a_vocs.pdf, last access: 29 April 2026.

Erisman, J. W., and Draaijers, G. P. J.: Atmospheric deposition in relation to acidification and eutrophication, Studies in Environmental Research 63, Elsevier, The Netherlands, 55–71, 1995.

Fares, S., Schnitzhofer, R., Jiang, X., Guenther, A., Hansel, A., and Loreto, F.: Observations of diurnal to weekly variations of monoterpene-dominated fluxes of volatile organic compounds from mediterranean forests: implications for regional modeling, Environ. Sci. Technol., 47, 11073–11082, https://doi.org/10.1021/es4022156, 2013.

Fuentes J. D. and Wang, D.: On the seasonality of isoprene emissions from a mixed temperate forest, Ecol. Appl., 9, 1118–1131, https://doi.org/10.1890/1051-0761(1999)009[1118:OTSOIE]2.0.CO;2, 1999.

Fuentes, J. D., Wang, D., and Gu, L.: Seasonal variations in isoprene emissions from a boreal aspen forest, J. Appl. Meteorol. Climatol., 38, 855–869, https://doi.org/10.1175/1520-0450(1999)038<0855:SVIIEF>2.0.CO;2, 1999.

Geron, C., Guenther, A., Sharkey, T., and Arnts, R. R.: Temporal variability in basal isoprene emission factor, Tree Physiol., 20, 799–805, https://doi.org/10.1093/treephys/20.12.799, 2000.

https://doi.org/10.5194/egusphere-2026-2550
Preprint. Discussion started: 26 May 2026

Guenther, A. B., Zimmerman, P. R., Harley, P. C., Monson, R. K., and Fall, R.: Isoprene and monoterpene emission rate variability: Model evaluations and sensitivity analyses, J. Geophys. Res., 98, 12609–12617, https://doi.org/10.1029/93JD00527Digital Object Identifier, 1993.

Guenther, A., Hewitt, C. N., Erickson, D., Fall, R., Geron, C., Graedel, T., Harley, P., Klinger, L., McKay, W. A., Pierce, T., Scholes, B., Steinbrecher, R., Tallamraju, R., Taylor, J., and Zimmerman, P.: A global model of natural volatile organic compound emissions, J. Geophys. Res., 100, 8873–8892, https://doi.org/10.1029/94JD02950, 1995.

Guenther, A. B., Karl, T., Harley, P., Wiedinmyer, C., Palmer, P. I., and Geron, C.: Estimates of global terrestrial isoprene emissions using MEGAN (Model of Emissions of Gases and Aerosols from Nature), Atmos. Chem. Phys., 6, 3181–3210, https://doi.org/10.5194/acp-6-3181-2006, 2006.

Guenther, A. B., Jiang, X., Heald, C. L., Sakulyanontvittaya, T., Duhl, T., Emmons, L. K., Wang, X.: The Model of Emissions of Gases and Aerosols from Nature version 2.1 (MEGAN2.1): an extended and updated framework for modeling biogenic emissions, Geosci. Model Dev., 5, 1471–1492, https://doi.org/10.5194/gmd-5-1471-2012, 2012.

Guenther, A. B.: Biological and chemical diversity of biogenic volatile organic emissions into the atmosphere, ISRN Atmospheric Sciences, 2013, 786290, http://dx.doi.org/10.1155/2013/786290, 2013.

Hata, H., Inoue, K., Yoshikado, H., Genchi, Y., and Tsunemi, K.: Impact of introducing net-zero carbon strategies on tropospheric ozone (O_3) fine particulate matter ($PM_{2.5}$) concentrations in Japanese region in 2050, Sci. Total Environ., 891, 164442, https://doi.org/10.1016/j.scitotenv.2023.164442, 2023.

Hayashi, K.: Atmospheric deposition 4. atmosphere-land exchange of substances, J. Jpn. Soc. Atmos. Environ. 45, A21-A31, 2010.

Holzinger, R., Lee, A., McKay, M., and Goldstein A. H.: Seasonal variability of monoterpene emission factors for a ponderosa pine plantation in California, Atmos. Chem. Phys., 6, 1267-1274, https://doi.org/10.5194/acp-6-1267-2006, 2006.

Ieda, T., Kitamori, Y., Mochida, M., Hirata, R., Hirano, T., Inukai, K., Fujinuma, Y., and Kawamura, K.: Diurnal variations and vertical gradients of biogenic volatile and semi-volatile organic compounds at the Tomakomai larch forest station in Japan, Tellus. Ser. B, Chem. Phys. Meteorol., 58, 177–186, https://doi.org/10.1111/j.1600-0889.2006.00179.x, 2006.

Ichikawa, Y., Nojiri, K., and Sasaka, K.: Determination of BVOCs based on high time-resolved measurements in urban and forest areas in Japan, Asian j. atmospheric environ., 17, 10, https://doi.org/10.1007/s44273-023-00009-6, 2023.

IPCC: https://www.ipcc.ch/report/ar6/wg1/, last access: 29 April 2026.

Japan Meteorological Agency: https://www.jma.go.jp/jma/press/2509/05b/kentoukai20250905.html, last access: 29 April 2026.

Jutti, S.: Monoterpene emission rate measurements from a Monterey Pine, J. Geophys. Res., 95, 7515-7519, https://doi.org/10.1029/JD095iD06p07515, 1990.

Kramshøj, M., Vedel-Petersen, I., Schollert, M., Rinnan, Å., Nymand, J., Ro-Poulsen, H., & Rinnan, R.: Large increases in Arctic biogenic volatile emissions are a direct effect of warming, Nat. Geosci., 9, 349–352, https://doi.org/10.1038/NGEO2692, 2016.

https://doi.org/10.5194/egusphere-2026-2550
Preprint. Discussion started: 26 May 2026

Kuzma, J., and Fall, R.: Leaf isoprene emission rate is dependent on leaf development and the level of isoprene synthase, Plant Physiol., 101, 435–440, https://doi.org/10.1104/pp.101.2.435, 1993.

Langford, B., Cash, J., Acton, W. J. F., Valach, A. C., Hewitt, C. N., Fares, S., Goded, I., Gruening, C., House, E., Kalogridis, A.-C., Gros, V., Schafers, R., Thomas, R., Broadmeadow, M., and Nemitz, E.: Isoprene emission potentials from European oak forests derived from canopy flux measurements: an assessment of uncertainties and inter-algorithm variability, Biogeosciences, 14, 5571–5594, https://doi.org/10.5194/bg-14-5571-2017, 2017.

Matsuda, K., Fujimura, Y., Hayashi, K., Takahashi, A., and Nakaya, K.: Deposition velocity of PM2.5 sulfate in the summer above a deciduous forest in central Japan, Atmos. Environ., 44, 4582–4587, https://doi.org/10.1016/j.atmosenv.2010.08.015, 2010.

Matsuda, K., Watanabe, I., Mizukami, K., Ban, S., and Takahashi, A.: Dry deposition of $PM_{2.5}$ sulfate above a hilly forest using relaxed eddy accumulation, Atmos. Environ., 107, 255–261, https://doi.org/10.1016/j.atmosenv.2015.02.050, 2015.

McKinney K. A., Lee, B. H., Vasta, A., Pho, T. V., and Munger, J. W.: Emissions of isoprenoids and oxygenated biogenic volatile organic compounds from a New England mixed forest, Atmos. Chem. Phys., 11, 4807–4831, https://doi.org/10.5194/acp-11-4807-2011, 2011.

McKinney, K. A., Wang, D., Ye, J., de Fouchier, J.-B., Guimarães, P. C., Batista, C. E., Souza, R. A. F., Alves, E. G., Gu, D., Guenther, A. B., and Martin, S. T.: A sampler for atmospheric volatile organic compounds by copter unmanned aerial vehicles, Atmos. Meas. Tech., 12, 3123-3135, https://doi.org/10.5194/amt-12-3123-2019, 2019.

Megaritis, A. G., Fountoukis, C., Charalampidis, P. E., Pilinis, C., and Pandis, S. N.: Response of fine particulate matter concentrations to changes of emissions and temperature in Europe, Atmos. Chem. Phys., 13, 3423–3443, https://doi.org/10.5194/acp-13-3423-2013, 2013.

Miyama, T., Okumura, M., Kominami, Y., Yoshimura, K., Ataka, M. and Tani A.: Nocturnal isoprene emission from mature trees and diurnal acceleration of isoprene oxidation rates near *Quercus serrata* Thunb. Leaves, J. For. Res., 18, 93–97, https://doi.org/10.1007/s10310-012-0350-5, 2013.

Mochizuki, T., Tani, A., Takahashi, Y., Saigusa, N., and Ueyama, M.: Long-term measurement of terpenoid flux above a *Larix kaempferi* forest using a relaxed eddy accumulation method, Atmos. Environ., 83, 53–61, https://doi.org/10.1016/j.atmosenv.2013.10.054, 2014.

Mochizuki, T., Miyazaki, Y., Ono, K., Wada, R., Takahashi, Y., Saigusa, N., Kawamura, K., and Tani, A.: Emissions of biogenic volatile organic compounds and subsequent formation of secondary organic aerosols in a Larix kaempferi forest, Atmos. Chem. Phys., 15, 12029–12041, https://doi.org/10.5194/acp-15-12029-2015, 2015.

Mochizuki, T., Takanashi, S., Wada, R., Miyazaki, Y., Nakano, T., & Tani, A.: Canopy fluxes of monoterpene, isoprene and isoprene oxidation products in a pine-oak forest. J. Agric. Meteorol., 76, 36–43. https://doi.org/10.2480/agrmet.D-19-00039, 2020.

Naemura, A., Yoshikawa, T., Satoh, K., and Dokiya, Y.: Measurements of throughfall and stem-flow of *Cryptomermeria japonica* in Oku-chichibu and Tama Hills. Jpn. J. Biometeror., 39, 121–125, https://doi.org/10.11227/seikisho.39.121, 2003.

https://doi.org/10.5194/egusphere-2026-2550
Preprint. Discussion started: 26 May 2026

Ninkovic, V., Markovic, D., and Rensing, M.: Plant volatiles as cues and signals in plant communication, Plant Cell Environ., 44, 1030–1043, https://doi.org/10.1111/pce.13910, 2020.

Nishimura, H., Shimadera, H., Kondo, A., Akiyama, K., and Inoue, Y.: Numerical analysis on biogenic emission sources contributing to urban ozone concentration in Osaka, Japan, Asian j. atmospheric environ, 9, 259–271, https://doi.org/10.5572/ajae.2015.9.4.259, 2015.

Okumura M, Tohno S, Tani A, Kominami Y, Miyama T, Takanashi S, and Kosugi Y: Isoprene emission characteristics of Quercus serrata in a deciduous broad-leaved forest. J. Agric. Meteorol., 64, 49–60, https://doi.org/10.2480/agrmet.64.49, 2008.

Okumura, M.: Environmental factors affecting the emission of volatile organic compounds from vegetation, Earozoru Kenkyu, 36, 19–24, https://doi.org/10.11203/jar. 36.19, 2021.

Penuelas, J., and Llusià, J.: Plant VOCs emissions: making use of the unavoidable, Trends Ecol. Evol., 19, 402–404, https://doi.org/10.1016/j.tree.2004.06.002, 2004.

Räisänen, T., Ryyppö, A., and Kellomäki, S.: Monoterpene emission of a boreal Scots pine (Pinus sylvestris L.) forest, Agric. For. Meteorol., 149, 808–819, https://doi.org/10.1016/j.agrformet.2008.11.001, 2009.

Rantala, P., Järvi, L., Taipale, R., Laurila, T. K., Patokoski, J., Kajos, M. K., Kurppa, M., Haapanala, S., Siivola, E., Petäjä, T., Ruuskanen, T. M., and Rinne, J.: Anthropogenic and biogenic influence on VOC fluxes at an urban background site in Helsinki, Finland, Atmos. Chem. Phys., 16, 7981–8007, https://doi.org/10.5194/acp-16-7981-2016, 2016.

Rasulov, B., Hüve, K., Bichele, I., Laisk, A., and Niinemets, Ü.: Temperature response of isoprene emission in vivo reflects a combined effect of substrate limitations and isoprene synthase activity: a kinetic analysis. Plant Physiol., 154, 1558–1570, https://doi.org/10.1104/pp.110.162081, 2010.

Seco, R., Karl, T., Turnipseed, A., Greenberg, J., Guenther, A., Llusia, J., Peñuelas, J., Dicken, U., Rotenberg, E., Kim, S., and Yakir, D.: Springtime ecosystem-scale monoterpene fluxes from Mediterranean pine forests across a precipitation gradient, Agric. For. Meteorol., 237, 150–159. https://doi.org/10.1016/j.agrformet.2017.02.001, 2017.

Sharifi, R., and Ryu, C. M.: Social networking in crop plants: wired and wireless cross-plant communications, Plant Cell Environ., https://doi.org/10.1111/pce.13966, 2020.

Sharkey, T. D., Wiberley, A. E., and Donohue, A. R.: Isoprene emission from plants: why and how, Ann. Bot., 101, 5–18, https://doi.org/10.1093/aob/mcm240, 2008.

Situ, S., Guenther, A., Wang, X., Jiang, X., Turnipseed, A., Wu, Z., Bai, J., and Wang, X.: Impacts of seasonal and regional variability in biogenic VOC emissions on surface ozone in the Pearl River delta region, China, Atmos. Chem. Phys., 13, 11803–11817, https://doi.org/10.5194/acp-13-11803-2013, 2013.

Tani, A., and Kawawata, Y.: Isoprene emission from the major native Quercus spp. in Japan, Atmos. Environ., 42, 4540–4550, https://doi.org/10.1016/j.atmosenv.2008.01.059, 2008.

Tani, A., and Mochizuki, T.: Review: Exchanges of volatile organic compounds between terrestrial ecosystems and the atmosphere, J. Agric. Meteorol., 77, 66–80, https://doi.org/10.2480/agrmet.D-20-00025, 2021.

https://doi.org/10.5194/egusphere-2026-2550
Preprint. Discussion started: 26 May 2026

Tani, A., Masui, N., Chang, T. W., Okumura, M., and Kokubu, Y.: Basal emission rates of isoprene and monoterpenes from major tree species in Japan: interspecies and intraspecies variabilities, Prog. Earth Planet. Sci., 11, 42, https://doi.org/10.1186/s40645-024-00645-8, 2024.

Wang, H., Nagalingam, S., Welch, A. M., Leong, C., Czimczik, C. I., and Guenther, A. B.: Heat waves may trigger unexpected surge in aerosol and ozone precursor emissions from sedges in urban landscapes, PNAS, 121, e2412817121, https://doi.org/10.1073/pnas.2412817121, 2024.

Wei, D., Fuentes, J.D., Gerken, T., Chamecki, M., Trowbridge, A. M., Stoy, P.C., Katul, G.G., Fisch, G., Acevedo, O., Manzi, A., von Randow, C, and dos Santos, R. M. N.: Environmental and biological controls on seasonal patterns of isoprene above a rain forest in central Amazonia, Agric. For. Meteorol., 256-257, 391–406, https://doi.org/10.1016/j.agrformet.2018.03.024, 2018.

Xu, M., Kasahara, K., Sorimachi, A., and Matsuda, K.: Nitric acid dry deposition associated with equilibrium shift of ammonium nitrate above a forest by long-term measurement using relaxed eddy accumulation, Atmos. Environ., 256, 118454, https://doi.org/10.1016/j.atmosenv.2021.118454, 2021.

Yang, W., Cao, J., Wu, Y., Kong, F., and Li, L.: Review on plant terpenoid emissions worldwide and in China, Sci. Total Environ., 787, 147454, https://doi.org/10.1016/j.scitotenv.2021.147454, 2020.

Yu, H., Guenther, A., Gu, D., Warneke, C., Geron, C., Goldstein, A., Graus, M., Karl, T., Kaser, L., Misztal, P., and Yuan, B.: Airborne measurements of isoprene and monoterpene emissions from southeastern U.S. forests, Sci. Total Environ., 595, 1498–1511, https://doi.org/10.1016/j.scitotenv.2017.03.262, 2017.